R. & M. No. 3747

PROCUREMENT EXECUTIVE; MINISTRY OF DEFENCE

AERONAUTICAL RESEARCH COUNCIL

REPORTS AND MEMORANDA

Low-Speed Wind-Tunnel Tests on some Slender Airbus Configurations

By D. A. Kirby and A. G. Hepworth

Aerodynamics Dept., R.A.E., Farnborough

LONDON: HER MAJESTY'S STATIONERY OFFICE

1974

PRICE £2·25 NET

Low-Speed Wind-Tunnel Tests on some Slender Airbus Configurations

By D. A. Kirby and A. G. Hepworth

Aerodynamics Dept., R.A.E., Farnborough

Reports and Memoranda No. 3747*
November, 1971

Summary

An experimental investigation has been made of the subsonic lift, drag and longitudinal stability characteristics of models representing some alternative slender airbus configurations. For the same wing planform of aspect ratio 1·4 the lift, drag and pitching moment have been measured for two wings of maximum thickness/chord ratio 4 and 9 per cent respectively, both without and with various body arrangements. Trailing-edge controls were cut on the 4 per cent wing and the results have been used to compare trimmed lift and drag coefficients for several alternative aircraft layouts. Included are the results of some tests with a foreplane which showed that considerable gains in usable lift coefficient and lift-drag ratio could be obtained with a high-foreplane low-wing configuration.

* Replaces R.A.E. Technical Report 71216—A.R.C. 33 488

LIST OF CONTENTS

1. Introduction

The possibilities of using the slender-wing concept for the design of a short-range airbus have been under discussion for some time[1,2] and work on layout studies[3] by Handley Page Ltd. under a Ministry contract had progressed to a more detailed design stage when the firm closed down. The original attraction of the slender wing stemmed from the prospect of achieving an extremely compact layout—one in which the passenger cabin is largely or entirely within the wing—which should facilitate obtaining low values of structure weight and cruise drag. More recently it has been realised[4,5] that siting the engines above wings of low aspect ratio offered an opportunity to obtain large reductions in the levels of aircraft noise experienced at ground level. A slender wing with engines placed above the centre region could therefore combine several worthwhile features; and the forward movement of the engines and propelling nozzles from the position near the trailing edge used for existing slender transport aircraft should allow some relief in the critical problem of balance and, hence, a wider choice of planform shape. Against a background of increasing legislation on aircraft noise and a consequent need to incorporate noise suppression qualities into the original design, the combination of overwing engines and a slender wing could therefore be attractive for several classes of aircraft and not just for the short-range airbus originally considered.

The precise form of aircraft layout will as usual depend on the number of passengers and the requirements of the airline operator and airworthiness authorities but the variations in cabin shape could be more extreme than for the classical aircraft with a separate wing and fuselage. For example, a large capacity would favour an all-wing design for a slender airbus since the requirements on head room could be met within an aerodynamic shape of good performance—perhaps having a supersonic cruise capability. With fewer passengers and hence a smaller aircraft, a smaller proportion of the plan area is available for passenger seating unless either some performance penalties are to be incurred by using a very thick wing[6] or some form of separate body is introduced. Depending on the capacity, and the aircraft's role, many aerodynamically integrated shapes with passengers shared between wing and forebody can be considered as alternatives to the more conventional arrangement where all the seats are in the fuselage and the wing is relatively thin.

Much of the slender-wing research work in the past has been concerned with isolated wings and currently experimental and theoretical work on cambered shapes which might be suitable for an all-wing layout is proceeding for both the low and high-speed regions of flight.[7] This Report is concerned only with low-speed characteristics and in particular with the effects of adding bodies to a wing of aspect ratio 1·4. It includes the results of tests on:-

(i) configurations where the body is of the same height as the wing maximum thickness but cross sectional shape and length are varied,

(ii) configurations where the body is circular in cross section and of large diameter compared with the wing thickness, i.e. it follows the classic aircraft form but has a slender rather than a swept wing and could be representative of 6, 8 or more abreast seating.

Details of the tests and descriptions of the various model arrangements are given in Section 2 of the Report. The relative merits of the 4 and 9 per cent thick wings and the effects of adding bodies are discussed in Section 3.

For subsonic transport aircraft the choice of wing and engine size is very dependent on the low-speed performance—landing governing the wing area and take-off the engine thrust—so, as is shown in Section 4, the tailless aircraft is at a disadvantage because of the large reductions in lift and large increases in drag arising from the use of trailing-edge controls to trim out the pitching moments associated with normal longitudinal stability. As an alternative trimming device the use of a foreplane is suggested for those configurations where a foreplane could be fitted well clear of the wing and the Report includes the results of tests in which the relative merits of high-wing low-foreplane and low-wing high-foreplane arrangements were investigated.

Finally in Section 5, several possible airbus layouts are compared on the basis of the trimmed lift and drag coefficients at low speed obtained for the simple configurations described in this Report.

2. Details of Models and Tests

The two wings tested were uncambered and had the same mild gothic planform defined by the equation

$$\frac{y}{s} = 0{\cdot}25\left\{5\left(\frac{x}{c_0}\right) - \left(\frac{x}{c_0}\right)^5\right\}$$

where s is the wing semispan, c_0 is the wing centreline chord and x and y are chordwise and spanwise distances respectively of the leading edge from the apex. The spanwise thickness distribution was of the form

$$\frac{z}{c_0} = \pm\frac{B(x)}{c_0}\left(1 - \frac{y^2}{s(x)^2}\right)$$

where z is the local half thickness, $s(x)$ is the local semispan and $B(x)$ is the local centreline half thickness defined by

$$\frac{B(x)}{c_0} = \frac{t}{c_0}\frac{x}{c_0}\left(1 - \frac{x}{c_0}\right)\left\{3{\cdot}2471 - 7{\cdot}5777\left(\frac{x}{c_0}\right) + 17{\cdot}8647\left(\frac{x}{c_0}\right)^2 - 19{\cdot}2073\left(\frac{x}{c_0}\right)^3 + 7{\cdot}6754\left(\frac{x}{c_0}\right)^4\right\}$$

and the maximum thickness chord ratio t/c_0 equalled either 9 or 4 per cent (Fig. 1).

The thicker wing $t/c_0 = 0{\cdot}09$ was tested with five different bodies all of which were symmetrical in thickness distribution and had a maximum thickness equal to t; so they did not extend beyond the point of maximum wing thickness at $x/c_0 = 0{\cdot}48$.* The narrowest body was of circular cross-section and consisted of a circular arc ogival nose of length $c_0/3$ ahead of the wing apex followed by a cylindrical portion of constant diameter t. The centre-line vertical section of this body was then retained for the other four bodies which covered variations in width, forebody length and planform shape (Fig. 2). These larger bodies all had elliptic cross-section shapes, the two largest having a maximum width of $3t$ which approximated very closely to one-third of a wing span and the body widths are given relative to the wing span in the figures. Full details of all the bodies are given in Table 1.

No controls were cut on the thicker wing but for the thinner wing ($t/c_0 = 0{\cdot}04$) plain trailing-edge flaps of constant chord equal to $0{\cdot}12c_0$ were represented over the whole span. These flaps were in three spanwise sections so that the effects of flap deflection could be tested with and without a body present. The two bodies made for the thinner wing were of circular cross-section over their whole length and consisted of an elliptic nose section of fineness ratio 1·5, a parallel portion of fineness ratio 5 and a rear body of fineness ratio 2·5 (Fig. 3). Compared with the bodies made for the thicker wing these large diameter bodies had a rounded nose and thus represented a later stage in the evolution of a practical body shape. The model was originally designed to represent a high-wing aircraft with an upswept rear end to give ground clearance, but the model was also tested inverted to represent a low-wing configuration and the rear body was not then a realistic shape. The wing was located in this body with its chordal plane parallel to the body centre-line and at a distance $t/2$ from the top or bottom of the body. The second body was axisymmetric and the wing was mounted on the body centreline. Both bodies extended $0{\cdot}4c_0$ ahead of the wing apex.

For both the high and low-wing configuration some tests were made with a foreplane. This consisted of a rectangular wing of N.A.C.A. 4415 section and aspect ratio 4, initially located fore and aft with its trailing edge at the wing apex. As the test programme developed the foreplane was first moved $0{\cdot}15c_0$ further forward and then fitted with a simple slotted flap. Either the upper or lower surface of the foreplane was flush with the body surface depending on which layout was being tested, *see* Fig. 3.

The various bodies and the foreplane were made from teak, but the 9 per cent wing was made of a resin-bonded glasscloth laminate sandwiched between two shaped teak sections and the 4 per cent wing was made entirely of glasscloth and resin; the use of glasscloth allowed the leading edges to be better defined and less fragile than if teak had been used throughout.

For the force and moment tests the models were hung by means of the normal wire rig from the overhead balance of the 4 ft × 3 ft wind tunnel at Farnborough. With the exception of some of the test runs with a foreplane, all the runs were made over an angle of incidence range from $\alpha = -5$ to 26 degrees at a speed of 60·8 m/s (199·5 ft/s) corresponding to a Reynolds number of $1{\cdot}97 \times 10^6$ based on the centreline chord. The transition on the wing was left free since previous work with sharp-edged slender wings in the 4 ft × 3 ft wind tunnel[6,8] had shown no advantage in fixing transition when the flow was dominated entirely by the leading-edge vortices. Transition was also left free on the bodies because at the low Reynolds number of 4 ft × 3 ft wind-tunnel tests large areas of roughness would be necessary to ensure a turbulent separation of the crossflow over the whole forebody length and in any case, the extent of the separation needed to represent a particular full-

* Because of the practical difficulties of manufacturing feather edges on the bodies to fit over the wing in a region where its thickness is changing slowly the body surface usually stopped well short of this point, *see* Fig. 10 for example.

scale condition was unknown. Some uncertainty must therefore be attached to the comparisons of the results with the various bodies on the thicker wing but probably only in the middle range of incidence since at high angles of incidence separation over the full forebody length will occur at full scale as on the models. The bodies on the thin wing were more blunt nosed than those on the thick wing so the flow separations were delayed to higher angles of incidence and had little influence on the forces—Section 3.3.1.

In non-dimensionalizing the results the wing-alone area and centreline chord were used for all the configurations. The effects of tunnel constraint were allowed for by the methods recommended in Ref. 9. Lift, drag and pitching moment coefficients for the wings are listed in Tables 2 and 3. The pitching moment coefficients are referred to a moment centre at mid centre-line chord, $0{\cdot}50c_0$.

In addition to the force and moment tests, surface flow patterns were obtained for some model configurations. The models were mounted on a sting rig and the patterns were produced by painting the model surfaces with a suspension of lampblack in kerosene increasing the wind speed quickly to the desired value, usually 30 m/s, and keeping it constant while the suspension dried. The resulting pattern was then photographed. A few of the photographs taken are presented in this Report—Fig. 10.

3. Discussion of Results with Controls Undeflected

3.1. Wings Without Bodies

Both the wings were tested without bodies and so the effects of changes in wing thickness for a mild gothic planform can be compared with the effects noted in Ref. 6 for a delta-wing planform.

3.1.1. *Lift and normal force.* Lift coefficients for the wings are shown in Fig. 4 and at low angles of incidence the loss in lift coefficient at constant incidence due to increasing wing thickness is very similar to that observed for the delta planform of Ref. 6. In detail the effect of changing a wing thickness depends on how the thickness distribution affects the contributions of the linear and non-linear components of the overall lifting force. For sharp-edged wings this distinction between the two components can conveniently be studied using the normal force coefficient, C_N; and, following the method of analysis adopted in Ref. 8, the normal force coefficient divided by the angle of incidence in radians is plotted against incidence, in order to determine the separate linear and non-linear contributions to the overall force, *see* Fig. 5. In this analysis the intercept of the curve with the C_N/α axis is regarded as the normal force arising from the linear flow field which, in slender body theory, is assumed to occur under attached flow conditions on the wing whilst the growth of C_N/α with increasing incidence shows how the non-linear force component, associated with the leading-edge vortices, develops.

For the 4 per cent wing the value of C_N/α at $\alpha = 0$ is very close to the value of 1·66 estimated using the correlation curve for 4 per cent wings derived in Ref. 8 for a wide range of planform shape. But, for the 9 per cent wing Fig. 5 shows that C_N/α at $\alpha = 0$ is in the region of 1·6; that is only 0·06 less than for the 4 per cent wing compared with a decrement in C_N/α of nearly 0·2 obtained previously[6] on delta wing for a 5 per cent change in thickness/chord ratio. Moreover the curves of C_N/α for the present two mild gothic wings are not so nearly parallel as the corresponding curves for the delta wings. A reduction in the non-linear contribution to C_N/α with increasing thickness was noted in the investigation of the effect of changing the edge-angle under conical flow conditions[10] and the work with alternative camber designs for the 9 per cent wing[7] has shown that both the linear and non-linear components are significantly affected by cross-section shape. Thus the precise form of the thickness distribution must have an influence and it is evident that more theoretical and experimental work is required before the differences in behaviour of the delta and mild gothic planform shapes can be rationalized.

At the higher angles of incidence both the 4 and the 9 per cent wings exhibit the type of break in the development of C_N/α (and C_m) with incidence which is always observed when the breakdown or bursting of the leading-edge vortices first occurs above a slender wing. Beyond this break the rate of increase of C_N/α with increasing angle of incidence is lessened as a larger area of the wing comes under the influence of the more diffuse rotational flow of the 'broken' form of the leading-edge vortices. The magnitude of the effect of this 'onset' of vortex breakdown on the lift coefficient of a slender wing depends on the proportion of the non-linear lift to the overall lift. When vortex breakdown occurs above the wings described in this Report only about one-third of the total lift is associated with the leading-edge vortices so the effects on the development of the overall lift coefficient with angle of incidence are not so marked as they would be for more slender wings. At the higher angles of incidence, however, there is a noticeable increase in the loss of lift coefficient due to increasing thickness because the onset of vortex breakdown occurs at a much lower incidence for the 9 per cent than for the 4 per cent wing. This result again conflicts with work on delta wings[11] where increasing thickness had little effect on the angle of incidence for the onset of vortex breakdown and highlights the lack of knowledge of the precise effect of planform and thickness variations on the vortex development.

3.1.2. *Drag and axial force.* Because of the increase in forward facing area as the wing thickness is increased the suctions induced by the leading-edge vortices on the upper surface of the wing produce a larger thrust force for the 9 per cent than for the 4 per cent wing, *see* Fig. 6. As was shown in Ref. 6, the effect of changes in thickness on the overall drag depends on the interplay between terms arising from the resolution of the normal and axial forces. The lift-dependent drag factor can be approximated[6] as

$$K = \frac{\pi A}{C_L}\left(\tan\alpha - \frac{C_{D_0} - C_A}{C_N}\right),$$

and at low and moderate angles of incidence and lift coefficient the reduction in $(C_A - C_{D_0})$ with increasing thickness outweighs the concurrent increase in tan α resulting from the lower lift slope of the thicker wing, Fig. 4. At higher lift coefficients the advantage of increasing thickness is lessened because the change in tan α becomes larger—Ref. 6. For the present two wings, because vortex breakdown occurs earlier on the 9 per cent wing than on the 4 per cent wing very large changes in the value of tan α for a constant lift coefficient begin to occur at about $C_L = 0{\cdot}6$ and above this value of lift coefficient the lift-dependent drag of the thicker wing is greater than that of the thinner wing, Fig. 7. In calculating the values of the factor K plotted in Fig. 7, the values of C_{D_0} used are derived from the drag polars ignoring the localized laminar-drag bucket which occurs at incidences near zero—Fig. 6 and Tables 2 and 3.

3.1.3. *Pitching moment.* Pitching moment coefficients about the moment axis at $0{\cdot}50c_0$ are compared for the two wings in Fig. 8. Kinks in the curves indicate that vortex breakdown crosses the trailing edge at about $\alpha = 14$ degrees and 20 degrees for the 9 per cent and 4 per cent thick wings respectively.

The aerodynamic centre position relative to the wing apex, x_n, has been calculated from the expression

$$x_n = \left(0{\cdot}50 - \frac{\partial C_m}{\partial C_N}\right)c_0$$

and the results are plotted in Fig. 9. The aerodynamic centre is further aft on the thicker wing over the whole range of lift coefficient with the exception of a limited region where vortex breakdown first affects the 9 per cent thick wing. For a wing at zero lift coefficient the aerodynamic centre is coincident with the centre of pressure and this can be estimated using slender-wing theory by the method given in Appendix B of Ref. 8. Measured and estimated values are as shown in Table 4.

The $0{\cdot}04c_0$ discrepancy between the estimated and measured values is consistent with that reported in Ref. 8 for several wing planforms and reflects the inadequacy of the theory to predict the loading near the trailing edge correctly.

With increasing lift coefficient the aerodynamic centre first moves rearward but, as explained in Ref. 8, for all slender wings the forward movement of the centre of action of the non-linear component of lift with increasing incidence causes a pitch-up tendency to develop at the higher lift coefficients. For planforms of the gothic type the pitch up is very mild and can be obscured by irregularities in the pitching moment arising from changes in the position of the secondary vortex separation on the wing upper surface and from the movement of vortex breakdown ahead of the wing trailing edge—for an example of the former *see* Fig. 6 of Ref. 8 and for the latter Fig. 8 of this Report. The onset of vortex breakdown was responsible for the largest irregularity in the development of the pitching moment coefficient with lift coefficient on both the 4 and 9 per cent wings; but for the 9 per cent wing the rapid changes in aerodynamic-centre position occur in the range of incidence which is likely to be used during approach and landing. Thus, although the kink in the pitching moment curve is small, this particular combination of wing shape and thickness should not be used in practice for an aircraft configuration. For the 4 per cent wing the kink occurs outside the normal usable range of incidence but it might set a limit on the maximum allowable angle of incidence and hence from airworthiness considerations on the approach speed.

3.2. Effect of Adding Bodies to the 9 per cent Thick Wing

3.2.1. *Flow visualization.* Observations of the flow over the upper surface of the wing and all five bodies were made at angles of incidence of 0, 5, 10, 15, 20 and 25 degrees. For the wing the sharp leading edges ensured a flow separation at the leading edge for all angles of incidence other than zero but for all the bodies the flow over the surface remained attached until beyond $\alpha = 5$ degrees. The surface flow patterns at 10 degrees indicated that the flow had separated from the sides of the bodies and created weak vortices which passed

downstream over the centre region of the wing; (for example *see* Fig. 10a). At $\alpha = 10$ degrees these vortices were most noticeable with the largest body, presumably because this had the thinnest cross-sectional shapes and the flow separated at a lower incidence than for the more circular bodies. As the angle of incidence was increased beyond 10 degrees the body vortices strengthened for all sizes of forebody but the angle of incidence at which the surface flow patterns indicated that the body and wing vortices were coalescing naturally depended on the lateral spacing of the body and wing vortex systems. Thus for the largest body, $w_B/b = \frac{1}{3}$, at $\alpha = 15$ degrees the trailing body vortices had swung towards the stronger wing leading-edge vortices, whereas for the $w_B/b = \frac{2}{9}$ body, the two systems were still some distance apart (*cf.* Figs. 10b and c). By $\alpha = 25$ degrees only the surface flow patterns on the wing with the smallest body showed a clear demarcation between the wing and body vortices, and, for the larger bodies the vortex system was becoming very similar to that on a wing of ogee planform, Fig. 10d.

3.2.2. *Lift.* Curves of lift coefficient against angle of incidence are shown for the wing alone and the wing with each of the five bodies in Fig. 11. The effect on the overall lift coefficient of adding a body is small until the flow around the body separates but when this happens a marked non-linear lift is developed on the forebody and substantial increases in lift coefficient occur at the higher incidences when the forebody is large. Fig. 12 shows the relationship between increases in lift and the increase in plan area for angles of incidence of 15, 20 and 25 degrees.

Varying body width changes the strength of the body vortices, affects the length of wing leading-edge shedding vortices and may affect the vortex breakdown characteristics so no general rule can be deduced from Fig. 12. Only at $\alpha = 25$ degrees where the flow has become similar to that on an ogee wing is a steady increase of lift with increase in plan area noticeable.

3.2.3. *Drag.* At the lift coefficients appropriate to take-off and landing conditions, the drag is nearly all lift-dependent and the lift-dependent drag factor is plotted in Fig. 13 for all the configurations tested with the 9 per cent thick wing. At low lift coefficients all the bodies caused increases in lift-dependent drag but at higher angles of incidence, where the flow round the forebodies had separated and produced large gains in lift coefficient, there was a considerable reduction in the drag at constant lift because of the reduction in the $C_L \tan \alpha$ term which dominates the drag at high incidence—*see* Ref. 6.

3.2.4. *Pitching moment.* Pitching moment coefficients are plotted against lift coefficient in Fig. 14 which shows separately the effects of length, width and shape variations in the forebody. For all the configurations, the addition of the body caused a nose up moment and this destabilizing effect was very large for the two wide bodies even before the flow over the body had separated.

Aerodynamic-centre positions for the 9 per cent wing with various bodies are shown in Fig. 15. The curves are shown dotted for those values of lift coefficient where the occurrence of vortex breakdown above the wing causes severe kinks in the curves of pitching moment against lift coefficient. In Ref. 8 it was noted that the forward movement in aerodynamic-centre position at constant lift coefficient caused by adding a body, reduced with increasing lift as long as the flow over the forebody remained attached, because with a body present the point of action of the non-linear component of the lift on the wing was moved rearwards—the leading-edge vortices starting at the wing-body junction rather than the wing apex. A similar effect can be seen in Fig. 15. For the largest body the reduction in Δx_n, the change in aerodynamic-centre position resulting from the addition of a body, between $C_L = 0$ and 0·2 was $0{\cdot}25c_0$.

At zero lift, for symmetrical configurations, the aerodynamic centre is coincident with the centre of pressure in attached flow, and this can be estimated by using slender wing and body theory[12] to calculate the loading distribution. Comparisons between measured and estimated values for the wing with the three forebodies of length $f_B/c_0 = \frac{1}{3}$ and partly parallel planforms are given in Table 5.

Most of the discrepancy between theory and experiment arises from the failure to predict the wing-alone loading correctly as mentioned earlier in Section 3.1.3.

3.3. Effect of Adding Bodies to the 4 per cent Thick Wing

Some difficulty was experienced in setting the trailing-edge control of the 4 per cent wing to particular angles and for the work aimed at investigating the effect of trailing-edge deflection the control angle was measured after setting, *see* Section 4*. With the bodies added to the wing to give the mid and high-wing

* In order to avoid spoiling the wing surface the flaps were held by alternative pieces of bent plate inserted as a tongue between grooves in the wing and flap. Tightening the holding screws caused movements which because of the small scale were not negligible.

configurations the nearest control angles to zero which could be obtained were +0·3 and −0·6 degree respectively, so the values of lift drag and pitching moment coefficient given in Table 6 have been used to give data for zero deflection before plotting in Figs. 16–19 for comparison with the low-wing configurations where zero control deflection was achieved directly.

3.3.1. *Lift.* Comparing the developments of the lift coefficient as the angle of incidence is increased, for the three wing-body configurations, with that of the wing alone in Fig. 16, shows a reduction in slope whereas the bodies on the thick wing discussed in Section 3.2 and other bodies in Ref. 8 caused no loss of lift compared with the wing-alone tests. Observations of the surface flow were made at $\alpha = 15$ degrees for the low-wing configuration and showed no evidence of disturbances in the wing-body junction region and a normal development of the leading-edge vortices. Even at this comparatively high incidence however, separation of the cross-flow past the body had only just started immediately in front of the wing and there was no evidence of body vortices above the elliptic nose. It is therefore concluded that there was insufficient forebody lift to offset the loss in wing lift arising from the restriction in length of the leading-edge vortices when the large-diameter body was added.

Because the model with an offset wing was designed originally to represent a high-wing aircraft and then inverted to provide information on a low-wing design, any effects on the lift caused by wing-body interference and/or rear-body shaping will rotate with the model. Thus, compared with the mid-wing configuration, the high and low-wing positions show differences in lift coefficient at zero incidence which are equal but opposite in sign, Fig. 16. In order to resolve whether this difference was caused by the rear-body shaping directly, or by its proximity to the wing, a further test was made in which the cylindrical part of the body was extended by 1·67 diameters so that the asymmetry of the rear body began at, and not ahead of, the wing trailing edge. The results of this test are given in Table 7 and they show, as did the tests without a wing discussed later in Section 4.2, that the effect of the rear-body shaping by itself was very small and that it was only in conjunction with the wing that the comparatively large changes in lift and pitching moment coefficient observed can occur. Unfortunately this means that the gain in lift coefficient relative to the mid-wing configuration measured on the low-wing model is associated with a geometry which, because of ground clearance problems during landing and rotation at take-off, is unlikely to be a practical proposition. Further work to understand the interference between the rear body and the wing and to minimize the possible losses in lift coefficient is clearly desirable.

3.3.2. *Drag.* The lift-dependent drag factors $(C_D - C_{D_0})/(C_L^2/\pi A)$ for the three wing positions are compared with those for the wing alone in Fig. 17. Because, in addition to a laminar-drag bucket at low angles of incidence, there were for the tests with bodies asymmetries in the drag polars arising from offset body effects or small control angles, the values of C_{D_0} for these tests could not be defined so accurately as for the test with the wing alone, but the errors are small compared with the total drag coefficients at incidences applicable to take-off and landing conditions. The values of C_{D_0} used in Fig. 17 were 0·0076 for the wing alone, 0·0120 for the mid-wing and 0·0125 for the low and high-wing configurations.

At a constant lift coefficient the lowest drag was obtained with the low-wing position and up to $C_L = 0{\cdot}8$ the lift-dependent drag factor calculated relative to $C_L = 0$ for the low-wing model was even smaller than that of the wing alone. This cannot however be regarded as a true comparison because, as discussed previously, the changes in lift coefficient associated with turning the model over are unlikely to be obtained on practical configurations. A more valid starting point for a drag comparison is therefore provided by Fig. 17b where the lift-dependent drag factors are considered relative to the C_L (= +0·015 for the low-wing, 0 for the mid-wing and −0·15 for the high-wing position) for minimum drag (= C_{D_0} within the experimental accuracy). In this presentation the factors are much closer and always higher than for the wing alone. This behaviour is in keeping with that obtained at low lift coefficients for the various bodies on the thick wing discussed in Section 3.2; but for higher lift coefficients the addition of those bodies yielded lower lift-dependent drag factors than the thick wing alone because the separated flow on the bodies allowed a reduction in the angle of incidence needed for a given lift coefficient, i.e. a reduction in the $C_L \tan \alpha$ term mentioned earlier.

3.3.3. *Pitching moment.* Comparison of the pitching moment coefficients at zero incidence for the various models shows that the combined effect of rear-body shaping and offset wing position causes an increment $\Delta C_m = \pm 0{\cdot}009$ at $\alpha = 0$ degree, (Fig. 18). For the high wing position the model was a practical shape and the nose-up pitching moment which resulted is beneficial since it will reduce the loss in lift coefficient incurred in trimming—assuming an aircraft with a positive static margin and using trailing-edge controls or a tailplane. The rear shape of the low-wing model is not realistic so the further decrement implied by the nose-down pitching moment at zero incidence need not apply in practice. As for the lift (discussed in Section 3.3.1), the further test with an extended body length showed that most of the change in pitching-moment coefficient at zero incidence stemmed from an interference effect and not from the body shape alone (*see* Table 7).

For all three body positions the addition of the body was destabilizing overall but there was no tendency to 'pitch up' at high angles of incidence because the bodies did not develop non-linear lift to any extent; compare the bodies on the thick wing discussed in Section 3.2.2. At low lift coefficients about 2 per cent c_0 forward shift in aerodynamic centre was obtained when the body was added for all three configurations (Fig. 19). Small irregularities in pitching-moment development made the effect more random at higher lift coefficients and the positions of the kinks in the pitching-moment curves show that the incidence at which vortex breakdown first affected the wing varied between configurations. With a high wing the phenomenon appeared to be avoided altogether over the range of incidence tested.

4. Control Effects and the Use of a Foreplane to Increase Usable Lift Coefficient

4.1. Effect of Deflecting Trailing-Edge Controls

The full-span controls fitted to the 4 per cent wing alone were tested over a range of control deflection from $\eta_{\text{nominal}} = -10$ to $+20$ degrees. The results are listed in Table 8 and plotted in Figs. 20–23. Except for the maximum control angle at high angles of incidence, the variations of lift and pitching-moment coefficient with control angle were linear and the control powers plotted in Fig. 24 could be accurately defined. Examination of the curves of pitching-moment coefficients plotted in Fig. 22 shows that there is little effect of control angle on the angle of incidence at which vortex breakdown affects the flow over the wing so higher lift coefficients can be realized without vortex breakdown when controls are deflected downwards, *see* Fig. 23. However, when the break in the pitching-moment curve does occur, it is more severe.

Control powers varied as the angle of incidence was increased but at attitudes typical of the take-off and landing phases of flight, $\partial C_L/\partial\eta$ was about 1·3 and $\partial C_m/\partial\eta$ about 0·4 per radian. The results of calculations of the point at which the increment in lift due to control deflection acts are given in Table 9 and demonstrate that this increment is centred on $0{\cdot}78c_0$ over a wide range of incidence and is consequently acting $0{\cdot}10c_0$ ahead of the control hinge line at $0{\cdot}88c_0$.

Some of the tests with control angle deflected were repeated for two wing-body configurations, $\eta_{\text{nominal}} = 0$, 10 and 20 degrees for the high wing and $\eta_{\text{nominal}} = 0$, 5 and 10 degrees for the low wing. The controls extended over only 83 per cent of the wing span for these tests so the control powers shown for zero angle of incidence in Fig. 24 are less than for the wing alone.

Because of interactions between the flow fields of the controls and the rear body variation of the lift and pitching moment with control deflection is not so straightforward when the body is present, but the point of action of the increment in lift due to control deflection remains in much the same position, *see* Table 9.

The effect of control deflection on drag, illustrated by Fig. 21, shows that considerable reductions in drag at constant lift can be obtained when the controls are deflected downwards, that is, when the $C_L \tan\alpha$ component of the overall drag is reduced. At a take-off lift coefficient of, say, 0·5 up to 20 per cent reductions in wing drag are possible if the need for up elevator to trim the aircraft can be avoided.

4.2. Use of a Foreplane

For tailles aircraft the use of trailing-edge devices to trim out the nose-down pitching moment associated with conventional stability criteria can result in substantial losses in the overall available lift coefficient since the point of action of the change in lift due to a control movement acts at such a short distance behind the CG. The effective moment arm of the controls discussed in the previous section was only about one-third of the centreline chord. Accepting that some degree of longitudinal stability is still required,* there could therefore be considerable advantages in employing a device ahead of the CG to trim the aircraft and if the device has sufficient high-lift capability then further increases in trimmed lift coefficient could be obtained by introducing a trailing-edge flap. Also, since, as shown in Section 4.1, downwards deflection of the trailing edge gives reductions in the drag for a constant lift, better take-off and climb performance should be obtained.

The use of a foreplane to provide the pitching moment to trim the aircraft has been considered during the initial design stages of many aircraft in the past but has rarely reached the hardware stage because the complex interference between the flow fields of the foreplane and of the wing and fin usually gives rise to major longitudinal, lateral and directional stability problems. Moreover it can be shown[13] that to be of reasonable size the foreplane must be capable of achieving a maximum lift coefficient which is higher than that possible on the

* If the aircraft is balanced in the unstable sense, that is with the CG aft of the aerodynamic centre, then downwards control deflection can be used for trimming and the benefits in lift and drag indicated by Figs. 20 and 21 can be enjoyed. To do this requires the development of an autostabilization system of absolute integrity acceptable to the airworthiness authorities.

mainplane, so it is unsound to expect to gain an advantage for the type of layout where the wing is operating near the limits of the current state of the art in the provision of high lift.

If, however, a medium-high aspect ratio wing with high-lift devices is used as a foreplane in front of a wing of comparatively low-wing loading, such as the slender wing of a 'quiet airbus' configuration, then the drawbacks might be lessened. To investigate the potentialities of such a layout some preliminary tests have been made with a foreplane of rectangular planform and aspect ratio 4, mounted as far from the wing-plane in height as possible on the wing-body model, in both its high- and low-wing configurations, Fig. 3. The aerofoil section of the foreplane was chosen as N.A.C.A. 4415 to give good high-lift characteristics at the low Reynolds number of the tests. Lift and pitching-moment coefficients for the tests with foreplane are plotted in Figs. 25 to 27.

Observations of the flow over the model with the high wing and low foreplane positions showed that as the angle of incidence was increased the trailing vortices shed by the foreplane moved towards the wing and at some critical incidence, depending on the foreplane setting, came more directly under the influence of the wing flow field. As a consequence the trailing vortices at this point flicked onto the upper surface of the wing and wrapped round its leading-edge vortices. When this happened the lift of the combined wing and foreplane model fell below that of the wing and body without foreplane and the pitching moment characteristic became very non-linear, Figs. 25 and 27a.

In contrast, with the model inverted, that is representing an aircraft with a low wing and a high foreplane, the trailing vortices from the foreplane moved away from the wing as angle of incidence was increased. Observations at the trailing edge of the wing, with the foreplane set at $\eta_F = 0$ degree, showed that the distance between the centres of the foreplane vortices and the wing increased from three quarters of a body diameter at $\alpha = 0$ degree to about two body diameters at $\alpha = 15$ degrees whilst the centre of the wing leading-edge vortices only rose about half a body diameter, i.e. the gap between the two vortex systems doubled. Because of this spacing, the lift and pitching moment coefficients exhibit a much more regular behaviour with increasing foreplane setting than was shown with the high wing and low foreplane, Figs. 25 to 27; and loss of lift results only when the foreplane stalls which naturally occurs at an earlier model incidence as η_F is increased.

The greater effectiveness of the low-wing high-foreplane combination is demonstrated quite strikingly in Fig. 27 by the values of CG position which were necessary to give zero static-stability margin at low lift coefficients.

Following these tests showing the superiority of the low-wing high-foreplane configuration, attempts were made to improve the contribution of the foreplane: (a) by moving it forward to increase the moment arm, and (b) by fitting it with a simple slotted flap at the trailing edge. Comparing Figs. 27 and 28 shows that both of these modifications increased the nose up moment but the increment was still insufficient to trim the model with trailing-edge controls deflected 10 degrees. By reducing the deflection to 5 degrees a condition was obtained in which the chosen foreplane provided enough nose-up moment to ensure trim at low lift coefficients with some margin for control and for forward movement of the CG. For this configuration all the lift drag and pitching moment coefficients are presented in Figs. 29–31, and the data has been used in making the comparisons of trimmed lift and drag coefficients for alternative airbus configurations in Section 5.

Even with the slotted flap the foreplane had insufficient high-lift capability to provide adequate control beyond about $C_L = 0{\cdot}6$ whereas, to satisfy the design requirements for an aircraft, trim with the most forward CG positions should be demonstrable up to lift coefficients at least 50 per cent greater than those used operationally, i.e. to about $C_L = 1{\cdot}2$ for the layout tested where $C_L = 0{\cdot}8$ could be obtained at the likely maximum allowable landing incidence of, say, $\alpha = 15$ degrees.

In order to determine the operating loads on the high foreplane in more detail a few tests were made without the wing, using a circular bar suspended from the normal wire rig in the 4 ft × 3 ft wind tunnel to support the body. These tests showed that the maximum lift coefficient achieved by the foreplane was 1·3 based on its own gross plane area (0·13 on the wing area). Only 45 per cent of this lift increment was obtained for the complete model because of negative lift induced on the wing by the foreplane vortex system but the pitching moment of the combined system was up to 20 per cent more than that calculated from multiplying the foreplane lift by its moment arm.

To trim the present model with the moment centre at $0{\cdot}45c_0$ at a lift-coefficient of 1·2 with the existing foreplane would require a $C_{L_{foreplane}}$ of about 3. It was not feasible to achieve this on the small scale and Reynolds number of the 4 ft × 3 ft wind tunnel and further work on foreplanes has been done in the 13 ft × 9 ft wind tunnel at Bedford where six-component measurements are being made with a foreplane, having a high-lift system consisting of a slat and slotted flap, over a range of angle of incidence and sideslip on a model with a wing of aspect ratio 1·8. This will be the subject of a later report.

5. Comparison of Alternative Layouts and Concluding Remarks

For an aircraft of the airbus type which will have to be capable of landing at weights not much less than

the maximum take-off weight, the economic penalties attached to not achieving sufficient usable lift coefficient in the landing phase will be severe. Sizing of the engine and the determination of the take-off/cruise balance of the engine, hence its type, is very dependent on the drag of the aircraft in the second segment climb and low lift-dependent drag characteristics will be essential. Thus the relative values of the low-speed lift and drag coefficients of alternative configurations will have a large influence on the determination of a suitable layout.

In Fig. 32 values of trimmed lift and drag are compared for four of the alternative configurations represented by the models discussed in this report. No allowance is made for the effect of the addition of engines, fins, etc. on the lift or drag. These should not affect the lift particularly but the relative drag of the various configurations at zero lift would be changed slightly. The results in Fig. 32 are all based on the model Reynolds numbers and it should be noted that corrections for scale-effect are needed for proper comparisons on actual aircraft configurations of known size. Again, the relative drag of the various configurations would be changed at full-scale Reynolds numbers but as far as the low-speed performance is concerned the changes should be small in comparison with the lift-dependent drag.

The following configurations are compared in Fig. 32 for CG positions giving a longitudinal stability margin of roughly $0{\cdot}04c_0$ at lift coefficients in the range 0 to 1:

(i) the 9 per cent t/c_0 wing alone —representing an all wing aircraft.

(ii) the 9 per cent t/c_0 wing with a medium size forebody. —representing an aircraft with some passengers carried in a more conventional cabin.

(iii) the 4 per cent t/c_0 wing mounted in a high position a large diameter body. —representing an aircraft with a large diameter fuselage and permitting over-wing engines to be placed a long way from the wing edges, i.e. maximising the 'shadow' required for noise suppression.

(iv) the 4 per cent t/c_0 wing in a low position on the large body with a high foreplane. Wing trailing-edge flap $\eta = 5$ degrees. —evolved during the tests as a shape with conventional fuselage and good low speed performance but still allowing engines to be positioned some way from the wing edges.

In making these comparisons the effect of the rear-body shaping discussed in Section 3.3 has been eliminated. This may have slightly favoured the high wing aircraft because if in practice the body upsweep starts ahead of the wing trailing edge, as for the model tested, a lift penalty will be incurred. Consequently Fig. 32a may be regarded as showing broadly the same lift coefficient for the first three of the configurations described above with a clear advantage for the model with a foreplane. Subsidiary trends shown are that reductions in wing thickness increase the lift as also does the addition of a lifting forebody which encourages the formation of strong body vortices, but the latter could cause longitudinal stability problems at high angles of incidence.

The drag comparison reflects the importance on slender wing aircraft of reducing the angle of incidence at which a particular lift coefficient is achieved. The introduction of a foreplane permits such reductions in incidence for a given lift coefficient that the extra drag of the foreplane is more than counterbalanced by the decrease in lift-dependent drag. Thus, at the lift coefficients appropriate to take-off, substantial reductions in drag could be achieved.

All the wings tested for this Report were symmetrical and the degree of camber used to reduce the drag at cruise, and perhaps also at take-off, will obviously offset the comparisons made in Fig. 32. Some work with alternative camber designs for the 9 per cent t/c_0 wing has already been reported and further tests at both low and high speeds (up to $M = 1{\cdot}1$) have been completed for the 9 per cent t/c_0 wing with a camber designed to give attached flow at $C_L = 0{\cdot}1$. Work has also proceeded on camber shapes for the 4 per cent t/c_0 wing.

When the results of all these tests are analysed more realistic comparisons of alternative slender airbus shapes will be possible but the work described in the present Report has demonstrated the low-speed performance and longitudinal stability problems associated with several different layouts and shows that a considerable advantage could be gained by introducing a foreplane as a trimming device. For maximum benefit the foreplane should be positioned well above the wing and be retractable in the cruise phase of flight. Further work with a foreplane of a much higher lift capability than the one described in this Report has been done with a large model in the 13 ft × 9 ft tunnel at Bedford and the test programme included an assessment of the lateral and directional stability aspects which have in the past usually provided the main arguments against the use of foreplane.

LIST OF SYMBOLS

A	Aspect ratio
b	Overall span
C_A	Axial force coefficient
C_D	Drag coefficient
C_{D_0}	Drag coefficient at zero lift coefficient
C_L	Lift coefficient
C_N	Normal-force coefficient
C_m	Pitching-moment coefficient
c_0	Wing centre-line chord
f_B	Forebody length
K	Lift-dependent drag factor
l	Length of body
s	Wing semispan
$s(x)$	Local wing semispan
t	Maximum wing thickness
$B(x)$	Local centreline half thickness
w_B	Width of body
x_a	Distance of centre of area behind apex of wing
x_{CP}	Distance of centre of pressure behind apex of wing
x_n	Distance of aerodynamic centre behind apex of wing
z	Local half thickness
α	Angle of incidence
η	Angle of trailing-edge controls on the wing, positive when control deflected downwards
η_F	Foreplane angle relative to wing chordline

REFERENCES

No.	*Author(s)*	*Title, etc.*
1	G. H. Lee	Cheap short-range air transport: possibilities of cost reduction with all wing aircraft. *J. Royal Aero Soc.*, Vol. 69, pp. 744–749, November 1965.
2	D. Küchemann and J. Weber ..	An analysis of some performance aspects of various types of aircraft designed to fly over different ranges at different speeds. *Prog. in Aero Sci.* Vol. 9, 1968, pp. 329–456. R.A.E. Technical Report 66188, (A.R.C. 28369) (1966).
3	A. A. Blythe and J. B. Edwards ..	Layouts for 300 passenger slender wing short-haul aircraft. Handley Page Advance Project and Research Office Report 104, January 1969.
4	—	The quiet airbus. Rolls Royce T.S.D. 1693, August 1968.
5	E. G. Broadbent	The shielding of engine noise by an aircraft wing. R.A.E. Technical Report 70116 A.R.C. 32 422 (1970).
6	D. A. Kirby and D. L. I. Kirkpatrick	An experimental investigation of the effect of thickness on the subsonic longitudinal stability characteristics of delta wings of 70 deg sweepback. A.R.C. R. & M. 3673 (1969).
7	P. J. Butterworth	Low-speed wind-tunnel tests on a family of cambered wings of mild gothic planform of aspect ratio 1·4. A.R.C. C.P. No. 1163 (1970).
8	D. A. Kirby	An experimental investigation of the effect of planform shape on the subsonic longitudinal stability characteristics of slender wings. A.R.C. R. & M. 3568 (1967).
9	H. C. Garner, E. W. E. Rogers, W. E. A. Acum and E. C. Maskell	Subsonic wind-tunnel wall corrections. AGARDograph 109, October 1966.
10	D. L. I. Kirkpatrick	Investigation of the normal force characteristics of slender delta wings with various Rhombic cross sections in subsonic conical flow. A.R.C. C.P. No. 922 (1965).
11	P. B. Earnshaw	Measurements of the effects of thickness on vortex breakdown position on a series of sharp-edged delta wings. A.R.C. C.P. No. 1018 (1968).
12	B. Thwaites (ed.)	Incompressible aerodynamics. Fluid motion memoirs. Oxford University Press, 1960.
13	S. B. Gates	Notes on the tail-first aeroplane. A.R.C. R. & M. 2676 (1939).

TABLE 1

Details of Models

(a) *Wings*

Planform defined by	$\frac{y}{s}$	$= 0{\cdot}25\left\{5\left(\frac{x}{c_0}\right) - \left(\frac{x}{c_0}\right)^5\right\}$
Centreline chord	c_0	0·4717 m
Span	b	0·3810 m
Area	S	0·1048 m^2
Aspect ratio	A	1·385
Slenderness ratio	$\frac{s}{c_0}$	0·404
Centre of area	$\frac{x_a}{c_0}$	0·653
Maximum thickness	t	0·0426 and 0·0189 m
	$\frac{t}{c_0}$	0·0902 and 0·0400

Thickness distribution defined by equations given in Section 2.

(b) *Bodies added to 9 per cent thick wing*

Body plan shape	Body cross section shape	Length ahead of wing apex	Maximum width	Plan area of wing + body	Ratio of wing + body to wing area
Circular arc + constant width	Elliptic	0·0786 m	0·0852 m	0·1108 m^2	1·057
Circular arc + constant width	Circular	0·1572	0·0426	0·1100	1·050
Circular arc + constant width	Elliptic	0·1572	0·0852	0·1175	1·121
Circular arc + constant width	Elliptic	0·1572	0·1278	0·1268	1·210
Circular arc	Elliptic	0·1572	0·1278	0·1212	1·156

Centreline thickness distribution for all the bodies as for the circular body.

(c) *Bodies added to 4 per cent thick wing*

Diameter 0·0808 m

Overall length 0·7280 m

Wing body angle 0

Distance of body centreline from wing chordal plane

Low	Mid	High
0·0310 m	0	0·0310 m

Nose of bodies 0·1887 m ahead of wing apex ($0{\cdot}4c_0$).

Upsweep of rear body of the high wing model was 0·0202 m (0·25 body diameter).

TABLE 1—*continued*

(d) *Foreplane*

Centreline thickness distribution—N.A.C.A. 4415

Chord constant at	0·0508 m
Span	0·2032 m
Area	0·0103 m^2
Aspect ratio	4

Slotted flap chord = 0·0190 m (0·375 foreplane chord)

Foreplane located fore and aft
(i) with trailing edge of foreplane at wing apex.
(ii) with trailing edge 0·0708 m ($0·15c_0$) ahead of wing apex.

TABLE 2

Coefficients for Wing of $t/c_0 = 0{\cdot}09$

α_{deg}	C_L	C_D	C_N	C_A	$C_{m_{0.50}}$	$\frac{C_N}{\alpha}$	K
−4·77	−0·1565	0·0166	−0·1574	0·0036	0·00798	1·890	
−4·26	−0·1431	0·0154	−0·1438	0·0048	0·00670	1·935	
−3·74	−0·1195	0·0128	−0·1201	0·0050	0·00577	1·841	
−3·22	−0·1020	0·0114	−0·1025	0·0057	0·00485	1·823	
−2·70	−0·0802	0·0096	−0·0805	0·0059	0·00344	1·708	
−2·19	−0·0642	0·0086	−0·0645	0·0062	0·00255	1·690	
−1·67	−0·0492	0·0078	−0·0495	0·0063	0·00213	1·693	
−1·16	−0·0357	0·0068	−0·0358	0·0060	0·00186	1·766	$C_{D_0} =$
−0·65	−0·0211	0·0061	−0·0211	0·0059	0·00132	1·868	0·0072
−0·13	−0·0047	0·0059	−0·0047	0·0059	+0·00042	1·995	
+0·38	+0·0110	0·0059	+0·0110	0·0058	−0·00036	1·661	
0·89	0·0267	0·0064	0·0268	0·0059	−0·00169	1·716	
1·41	0·0452	0·0075	0·0454	0·0064	−0·00212	1·843	
1·92	0·0589	0·0084	0·0592	0·0065	−0·00233	1·763	
2·44	0·0752	0·0093	0·0756	0·0061	−0·00338	1·777	
2·95	0·0934	0·0105	0·0938	0·0057	−0·00438	1·819	
3·47	0·1097	0·0117	0·1102	0·0051	−0·00532	1·821	1·617
3·98	0·1272	0·0133	0·1278	0·0044	−0·00623	1·838	1·629
4·50	0·1455	0·0151	0·1462	0·0037	−0·00742	1·862	1·615
5·02	0·1704	0·0181	0·1714	0·0031	−0·00915	1·955	1·624
5·54	0·1881	0·0202	0·1892	0·0020	−0·01023	1·958	1·600
6·58	0·2294	0·0265	0·2310	+0·0001	−0·01278	2·013	1·594
7·61	0·2689	0·0335	0·2710	−0·0024	−0·01524	2·040	1·581
8·65	0·3110	0·0423	0·3138	−0·0049	−0·01788	2·079	1·577
9·74	0·3623	0·0546	0·3663	−0·0075	−0·02107	2·154	1·570
10·74	0·4077	0·0671	0·4131	−0·0101	−0·02403	2·205	1·566
11·77	0·4508	0·0803	0·4577	−0·0134	−0·02664	2·228	1·563
12·82	0·4969	0·0960	0·5059	−0·0166	−0·02904	2·262	1·564
13·86	0·5457	0·1149	0·5573	−0·0192	−0·03077	2·304	1·573
14.89	0·5848	0·1329	0·5993	−0·0219	−0·03118	2·305	1·598
15.93	0·6256	0·1525	0·6434	−0·0251	−0·03284	2·314	1·614
16.97	0·6702	0·1760	0·6924	−0·0273	−0·03531	2·338	1·635
18·01	0·7162	0·2016	0·7434	−0·0298	−0·03828	2·365	1·648
19.06	0·7624	0·2289	0·7953	−0·0326	−0·04129	2·392	1·659
20·10	0·8098	0·2565	0·8487	−0·0374	−0·04433	2·420	1·654
21·15	0·8679	0·2962	0·9163	−0·0369	−0·04880	2·482	1·669
22.20	0·9169	0·3321	0·9744	−0·0389	−0·05221	2·516	1·681
23·24	0·9650	0·3674	1·0317	−0·0432	−0·05517	2·544	1·683
24·28	1·0149	0·4089	1·0933	−0·0447	−0·05859	2·580	1·697
25·32	1·0539	0·4439	1·1425	−0·0494	−0·06108	2·585	1·711
26·36	1·1011	0·4879	1·2032	−0·0519	−0·06440	2·615	1·725

TABLE 3

Coefficients for Wing of $t/c_0 = 0{\cdot}04$

α_{deg}	C_L	C_D	C_N	C_A	$C_{m_{0.50}}$	$\frac{C_N}{\alpha}$	K
−4·63	−0·1562	0·0177	−0·1572	0·0050	0·00719	1·945	
−3·60	−0·1205	0·0137	−0·1211	0·0061	0·00548	1·927	
−2·56	−0·0820	0·0104	−0·0823	0·0067	0·00332	1·842	C_{D_0} =
−1·53	−0·0468	0·0085	−0·0470	0·0072	0·00160	1·760	0·0076
−0·50	−0·0156	0·0064	−0·0156	0·0062	+0·00035	1·788	
+0·52	+0·0166	0·0066	+0·0166	0·0065	−0·00084	1·829	
1·55	0·0471	0·0085	0·0474	0·0072	−0·00192	1·752	
2·58	0·0821	0·0102	0·0825	0·0065	−0·00366	1·832	
3·62	0·1238	0·0133	0·1244	0·0055	−0·00588	1·969	1·623
4·66	0·1661	0·0181	0·1670	0·0046	−0·00803	2·053	1·652
5·70	0·2093	0·0242	0·2107	0·0033	−0·01028	2·118	1·650
6·74	0·2553	0·0324	0·2574	0·0022	−0·01256	2·188	1·654
7·78	0·3023	0·0423	0·3053	+0·0009	−0·01497	2·248	1·652
8·82	0·3509	0·0541	0·3550	−0·0003	−0·01700	2·306	1·641
9·87	0·4003	0·0679	0·4060	−0·0017	−0·01913	2·357	1·638
10·91	0·4453	0·0817	0·4527	−0·0041	−0·02091	2·377	1·625
11·96	0·4966	0·0998	0·5065	−0·0052	−0·02302	2·426	1·627
13·01	0·5518	0·1206	0·5648	−0·0067	−0·02550	2·487	1·614
14·11	0·6074	0·1434	0·6240	−0·0090	−0·02823	2·534	1·601
15·10	0·6623	0·1692	0·6835	−0·0092	−0·03025	2·593	1·602
16·15	0·7122	0·1938	0·7380	−0·0120	−0·03176	2·618	1·597
17·19	0·7612	0·2196	0·7921	−0·0152	−0·03363	2·640	1·591
18·25	0·8198	0·2530	0·8578	−0·0165	−0·03578	2·693	1·589
19·29	0·8701	0·2846	0·9153	−0·0188	−0·03698	2·719	1·591
20·34	0·9237	0·3218	0·9780	−0·0193	−0·03790	2·755	1·602
21.38	0·9638	0·3543	1·0267	−0·0214	−0·03721	2·751	1·624
22·42	1·0097	0·3938	1·0836	−0·0211	−0·03776	2·769	1·648
23·47	1·0635	0·4388	1·1503	−0·0211	−0·04016	2·808	1·659
24·51	1·1092	0·4802	1·2084	−0·0232	−0·04272	2·825	1·671
25·55	1·1526	0·5221	1·2651	−0·0261	−0·04466	2·837	1·685
26·59	1·1948	0·5683	1·3228	−0·0266	−0·04730	2·850	1·709

TABLE 4

Centre-of-Pressure Position Relative to Wing Apex, x_{CP}/c_0

$\frac{t}{c_0}$	Measured at $C_L = 0$	Estimated by slender wing theory
0	—	0·563
0·04	0·530	0·571
0·09	0·539	0·580

TABLE 5

Centre-of-Pressure Position Relative to Wing Apex, x_{CP}/c_0

	Measured at $C_L = 0$	Estimated
Wing alone	0·539	0·580
$\frac{w_B}{b} = \frac{1}{9}$	0·533	0·575
$\frac{2}{9}$	0·517	0·562
$\frac{1}{3}$	0·475	0·535

TABLE 6

Coefficients for Wing of $t/c_0 = 0{\cdot}04$, with Bodies Added

α_{deg}	C_L	C_D	$C_{m_{0\cdot50}}$
High wing, $\eta = -0{\cdot}6$ deg			
−3·69	−0·1813	0·0238	0·01675
−2·66	−0·1473	0·0195	0·01527
−1·63	−0·1103	0·0162	0·01344
−0·60	−0·0746	0·0135	0·01211
0·43	−0·0427	0·0115	0·01227
1·46	−0·0128	0·0120	0·01180
2·49	+0·0202	0·0126	0·01119
3·52	0·0563	0·0143	0·01010
4·55	0·0935	0·0171	0·00922
5·59	0·1341	0·0216	0·00787
6·63	0·1771	0·0277	0·00625
7·67	0·2212	0·0352	0·00483
8·71	0·2666	0·0449	0·00328
9·75	0·3138	0·0562	0·00162
10·79	0·3602	0·0690	+0·00002
11·84	0·4086	0·0839	−0·00156
12·88	0·4572	0·1010	−0·00237
13·92	0·4980	0·1167	−0·00276
15·02	0·5534	0·1400	−0·00441
16·01	0·6019	0·1624	−0·00594
17·05	0·6495	0·1864	−0·00716
18·09	0·6915	0·2089	−0·00807
19·14	0·7474	0·2410	−0·01002
20·19	0·7963	0·2715	−0·01095
21·23	0·8472	0·3048	−0·01259
22·28	0·8986	0·3407	−0·01420
23·32	0·9489	0·3783	−0·01625
24·37	0·9963	0·4172	−0·01799
25·41	1·0420	0·4584	−0·02018
26·46	1·0921	0·5066	−0·02335

α_{deg}	C_L	C_D	$C_{m_{0\cdot50}}$
Low wing, $\eta = 0$ deg			
−4·62	−0·0994	0·0180	−0·00671
−3·58	−0·0612	0·0148	−0·00820
−2·55	−0·0258	0·0131	−0·00916
−1·53	+0·0018	0·0124	−0·00940
−0·50	0·0314	0·0114	−0·00936
+0·58	0·0622	0·0130	−0·01062
1·56	0·0961	0·0152	−0·01116
2·59	0·1331	0·0181	−0·01243
3·62	0·1711	0·0222	−0·01409
4·66	0·2119	0·0275	−0·01572
5·70	0·2547	0·0348	−0·01788
6·74	0·2970	0·0433	−0·01954
7·78	0·3441	0·0544	−0·02174
8·82	0·3920	0·0675	−0·02418
9·86	0·4392	0·0815	−0·02620
10·91	0·4873	0·0979	−0·02828
11·95	0·5355	0·1160	−0·03018
12·99	0·5834	0·1358	−0·03187
14·04	0·6351	0·1585	−0·03387
15·08	0·6818	0·1808	−0·03546
16·13	0·7348	0·2078	−0·03742
17·18	0·7853	0·2368	−0·03902
18·22	0·8304	0·2642	−0·04010
19·26	0·8768	0·2957	−0·04183
20·29	0·9133	0·3279	−0·04012
21·33	0·9514	0·3582	−0·04147
22·36	0·9928	0·3930	−0·04522
23·41	1·0389	0·4344	−0·04857
24·44	1·0765	0·4747	−0·05257
25·47	1·1036	0·5134	−0·05648

TABLE 6—*continued*

α_{deg}	C_L	C_D	$C_{m_{0\cdot50}}$
Mid wing, $\eta = +0\cdot3$ deg			
−4·66	−0·1495	0·0213	0·00306
−3·63	−0·1080	0·0169	0·00138
−2·59	−0·0678	0·0139	+0·00007
−1·56	−0·0373	0·0122	−0·00077
−0·54	−0·0088	0·0108	−0·00114
+0·49	+0·0239	0·0112	−0·00160
1·52	0·0573	0·0130	−0·00194
2·55	0·0897	0·0148	−0·00306
3·58	0·1240	0·0178	−0·00428
4·62	0·1637	0·0222	−0·00569
5·66	0·2071	0·0288	−0·00751
6·69	0·2476	0·0359	−0·00889
7·73	0·2940	0·0460	−0·01136
8·80	0·3415	0·0580	−0·01315
9·82	0·3899	0·0718	−0·01480
10·86	0·4367	0·0871	−0·01645
11·91	0·4860	0·1046	−0·01811
12·94	0·5284	0·1217	−0·01868
14·04	0·5817	0·1444	−0·02044
15·04	0·6353	0·1688	−0·02248
16·08	0·6747	0·1878	−0·02382
17·12	0·7286	0·2168	−0·02541
18·17	0·7788	0·2466	−0·02733
19·21	0·8227	0·2745	−0·02891
20·25	0·8634	0·2646	−0·02880
21·29	0·9159	0·3399	−0·03306
22·34	0·9680	0·3803	−0·03615
23·43	1·0128	0·4201	−0·03913
24·42	1·0548	0·4579	−0·04171
25·46	1·0969	0·4956	−0·04424
26·51	1·1471	0·5459	−0·04736

TABLE 7

Coefficients with Wing of $t/c_0 = 0\cdot04$ and Extended Body

α_{deg}	C_L	C_D	$C_{m_{0\cdot50}}$	α_{deg}	C_L	C_D	$C_{m_{0\cdot50}}$
Wing alone, $\eta = -0\cdot6$ deg				High wing with extended body, $\eta = -0\cdot6$ deg			
−4·70	−0·1856	0·0210	0·01325	−4·69	−0·1817	0·0263	0·01096
−3·66	−0·1453	0·0164	0·01112	−3·66	−0·1425	0·0213	0·00916
−2·63	−0·1068	0·0128	0·00906	−2·62	−0·1054	0·0177	0·00783
−1·59	−0·0666	0·0101	0·00710	−1·54	−0·0664	0·0151	0·00643
−0·51	−0·0309	0·0076	0·00581	−0·57	−0·0409	0·0134	0·00604
+0·47	−0·0036	0·0072	0·00491	+0·46	−0·0064	0·0124	0·00563
1·49	+0·0278	0·0087	0·00377	1·49	+0·0232	0·0138	0·00544
2·53	0·0635	0·0106	0·00230	2·52	0·0542	0·0151	0·00476
3·56	0·1013	0·0133	+0·00045	3·55	0·0931	0·0178	0·00364
4·65	0·1462	0·0181	−0·00178	4·59	0·1345	0·0219	0·00236
5·63	0·1825	0·0229	−0·00334	5·62	0·1724	0·0270	0·00102

TABLE 8

Coefficients for Wing of $t/c_0 = 0{\cdot}04$ with Trailing-Edge Controls Deflected

α_{deg}	C_L	C_D	C_m	α_{deg}	C_L	C_D	C_m
Control angle = −10·5 deg				Control angle = −5·2 deg			
				−3·74	−0·2306	0·0247	0·03535
				−2·70	−0·1903	0·0189	0·03265
				−1·67	−0·1511	0·0150	0·03042
				−0·63	−0·1149	0·0116	0·02823
				+0·40	−0·0814	0·0088	0·02649
1·32	−0·1705	0·0151	0·06068	1·42	−0·0507	0·0082	0·02591
2·35	−0·1369	0·0137	0·05793	2·45	−0·0170	0·0085	0·02424
3·38	−0·1018	0·0121	0·05601	3·49	+0·0199	0·0096	0·02268
4·41	−0·0633	0·0118	0·05403	4·52	0·0574	0·0117	0·02116
5·45	−0·0235	0·0130	0·05211	5·56	0·0990	0·0154	0·01963
6·49	+0·0179	0·0154	0·05047	6·65	0·1439	0·0211	0·01764
7·53	0·0636	0·0201	0·04854	7·64	0·1857	0·0277	0·01609
8·62	0·1120	0·0266	0·04676	8·73	0·2367	0·0375	0·01391
9·61	0·1534	0·0339	0·04520	9·72	0·2792	0·0471	0·01230
10·65	0·2028	0·0444	0·04345	10·77	0·3301	0·0606	0·01023
11·70	0·2522	0·0562	0·04196	11·86	0·3811	0·0758	0·00840
12·74	0·2976	0·0689	0·04061	12·85	0·4281	0·0912	0·00677
13·83	0·3479	0·0850	0·03926	13·90	0·4843	0·1116	0·00464
14·82	0·3934	0·1014	0·03845	14·95	0·5309	0·1308	0·00321
15·89	0·4422	0·1205	0·03757	16·00	0·5866	0·1554	0·00153
16·91	0·4907	0·1416	0·03605	17·10	0·6402	0·1818	+0·00012
17·96	0·5423	0·1665	0·03490	18·09	0·6883	0·2075	−0·00083
19·00	0·5953	0·1942	0·03264	19·14	0·7430	0·2394	−0·00207
20·10	0·6421	0·2206	0·03100	20·18	0·7885	0·2685	−0·00261
21·09	0·6868	0·2480	0·02823	21·22	0·8321	0·2989	−0·00355
22·14	0·7407	0·2843	0·02548	22·27	0·8872	0·3389	−0·00632
23·24	0·7947	0·3227	0·02321	23·31	0·9327	0·3742	−0·00803
24·22	0·8341	0·3520	0·02169	24·35	0·9788	0·4123	−0·00992
25·26	0·8785	0·3886	0·01983	25·45	1·0316	0·4596	−0·01275
26·30	0·9177	0·4254	0·01784	26·44	1·0750	0·5017	−0·01462

TABLE 8—*continued*

α_{deg}	C_L	C_D	C_m	α_{deg}	C_L	C_D	C_m
Control angle = −0·6 deg				Control angle = +5·2 deg			
−4·69	−0·1789	0·0205	0·01115	−4·57	−0·0460	0·0121	−0·02571
−3·65	−0·1392	0·0155	0·00912	−3·54	−0·0066	0·0099	−0·02729
−2·62	−0·0998	0·0118	0·00726	−2·50	+0·0291	0·0090	−0·02890
−1·59	−0·0619	0·0094	0·00520	−1·47	0·0643	0·0090	−0·03031
−0·56	−0·0292	0·0071	0·00395	−0·44	0·0982	0·0094	−0·03200
+0·47	+0·0030	0·0066	0·00281	+0·64	0·1314	0·0118	−0·03379
1·50	0·0342	0·0081	0·00162	1·62	0·1659	0·0156	−0·03547
2·53	0·0655	0·0095	+0·00063	2·65	0·2058	0·0199	−0·03842
3·57	0·1033	0·0120	−0·00125	3·74	0·2443	0·0256	−0·04028
4·60	0·1428	0·0161	−0·00325	4·73	0·2869	0·0326	−0·04259
5·64	0·1915	0·0223	−0·00570	5·77	0·3337	0·0417	−0·04518
6·68	0·2331	0·0293	−0·00778	6·86	0·3828	0·0531	−0·04764
7·72	0·2759	0·0377	−0·00957	7·85	0·4263	0·0647	−0·04950
8·76	0·3265	0·0494	−0·01189	8·90	0·4791	0·0802	−0·05227
9·81	0·3775	0·0631	−0·01423	9·89	0·5229	0·0948	−0·05407
10·85	0·4276	0·0781	−0·01629	10·99	0·5767	0·1138	−0·05650
11·90	0·4745	0·0939	−0·01790	12·03	0·6281	0·1355	−0·05887
12·94	0·5271	0·1132	−0·02012	13·08	0·6777	0·1560	−0·06075
14·00	0·5852	0·1367	−0·02257	14·13	0·7338	0·1824	−0·06328
15·04	0·6335	0·1582	−0·02421	15·18	0·7903	0·2110	−0·06554
16·09	0·6888	0·1850	−0·02620	16·22	0·8395	0·2380	−0·06696
17·14	0·7447	0·2148	−0·02801	17·28	0·8950	0·2710	−0·06891
18·19	0·7955	0·2432	−0·02934	18·33	0·9527	0·3075	−0·07081
19·29	0·8533	0·2787	−0·03095	19·37	1·0040	0·3418	−0·07236
20·28	0·8975	0·3100	−0·03062	20·42	1·0517	0·3775	−0·07312
21·31	0·9358	0·3417	−0·03026	21·45	1·0848	0·4103	−0·07060
22·41	0·9889	0·3829	−0·03190	22·48	1·1210	0·4457	−0·06962
23·40	1·0346	0·4212	−0·03375	23·52	1·1650	0·4861	−0·07060
24·44	1·0805	0·4613	−0·03588	24·56	1·2101	0·5292	−0·07220
25·48	1·1241	0·5029	−0·03793	25·61	1·2603	0·5807	−0·07426
26·58	1·1755	0·5548	−0·04026	26·65	1·3023	0·6273	−0·07624

TABLE 8—*continued*

α_{deg}	C_L	C_D	C_m	α_{deg}	C_L	C_D	C_m
Control angle = +9·8 deg				Control angle = +19·8 deg			
−4·48	0·0523	0·0117	−0·05224	−4·29	0·2691	0·0309	−0·11387
−3·45	0·0905	0·0114	−0·05377	−3·26	0·3058	0·0350	−0·11609
−2·42	0·1275	0·0127	−0·05546	−2·22	0·3481	0·0415	−0·11971
−1·33	0·1637	0·0141	−0·05817	−1·18	0·3864	0·0484	−0·12304
−0·36	0·1946	0·0170	−0·05988	−0·11	0·4126	0·0571	−0·12247
+0·68	0·2295	0·0215	−0·06244	+0·86	0·4404	0·0637	−0·12336
1·76	0·2704	0·0275	−0·06512	1·90	0·4777	0·0728	−0·12542
2·75	0·3101	0·0339	−0·06777	2·99	0·5272	0·0857	−0·12936
3·79	0·3527	0·0420	−0·07057	3·98	0·5662	0·0980	−0·13185
4·88	0·3965	0·0515	−0·07320	5·02	0·6138	0·1135	−0·13572
5·86	0·4385	0·0616	−0·07577	6·09	0·6602	0·1304	−0·13859
6·96	0·4909	0·0760	−0·07864	7·10	0·7067	0·1476	−0·14111
7·95	0·5340	0·0893	−0·08062	8·15	0·7578	0·1685	−0·14415
9·00	0·5854	0·1071	−0·08326	9·20	0·8117	0·1921	−0·14688
10·04	0·6387	0·1281	−0·08594	10·24	0·8583	0·2153	−0·14850
11·09	0·6914	0·1482	−0·08820	11·29	0·9094	0·2405	−0·15149
12·19	0·7446	0·1726	−0·09015	12·33	0·9615	0·2693	−0·15317
13·18	0·7935	0·1959	−0·09224	13·38	1·0110	0·3015	−0·15532
14·24	0·8527	0·2256	−0·09510	14·46	1·0709	0·3341	−0·15802
15·28	0·9026	0·2553	−0·09631	15·48	1·1232	0·3681	−0·15981
16·33	0·9541	0·2850	−0·09812	16·53	1·1749	0·4056	−0·16104
17·38	1·0095	0·3211	−0·10001	17·59	1·2197	0·4405	−0·16144
18·48	1·0678	0·3607	−0·10188	18·62	1·2705	0·4784	−0·16223
19·48	1·1193	0·3982	−0·10330	19·66	1·3221	0·5234	−0·16298
20·52	1·1664	0·4363	−0·10434	20·69	1·3470	0·5598	−0·15908
21·55	1·1990	0·4713	−0·10128	21·71	1·3710	0·5957	−0·15432
22·64	1·2358	0·5140	−0·09937				
23·62	1·2773	0·5564	−0·10025				
24·66	1·3205	0·6009	−0·10150				
25·70	1·3590	0·6439	−0·10220				
26·74	1·4016	0·6962	−0·10410				

TABLE 9

Control Powers for Wing of $t/c_0 = 0{\cdot}04$ without and with Bodies (Values per Radian)

α_{deg}	Wing alone			High wing on body			Low wing on body		
	$\frac{dC_L}{d\eta}$	$\frac{dC_m}{d\eta}$	$\frac{dC_m/d\eta}{dC_L/d\eta}$	$\frac{dC_L}{d\eta}$	$\frac{dC_m}{d\eta}$	$\frac{dC_m/d\eta}{dC_L/d\eta}$	$\frac{dC_L}{d\eta}$	$\frac{dC_m}{d\eta}$	$\frac{dC_m/d\eta}{dC_L/d\eta}$
0	1·203	0·346	0·288	0·951	0·285	0·300	0·819	0·234	0·286
2·5	1·203	0·349	0·290	0·968	0·293	0·303	0·894	0·246	0·275
5	1·230	0·355	0·289	1·020	0·303	0·297	0·917	0·261	0·285
7·5	1·249	0·359	0·287	1·060	0·315	0·297	0·974	0·268	0·275
10	1·289	0·367	0·285	1·094	0·321	0·293	0·974	0·269	0·276
12·5	1·341	0·370	0·276	1·100	0·312	0·284	0·968	0·268	0·277
15	1·375	0·376	0·273	1·112	0·313	0·281	0·963	0·274	0·285
17·5	1·415	0·382	0·270	1·049	0·308	0·294	0·923	0·271	0·294
20	1·404	0·382	0·272	1·008	0·285	0·283	0·917	0·264	0·288
22·5	1·335	0·351	0·263	0·980	0·278	0·284	0·917	0·249	0·272
25	1·209	0·342	0·283	0·945	0·275	0·291	0·894	0·215	0·240

Note: Pitching moment centre at $0{\cdot}50c_0$

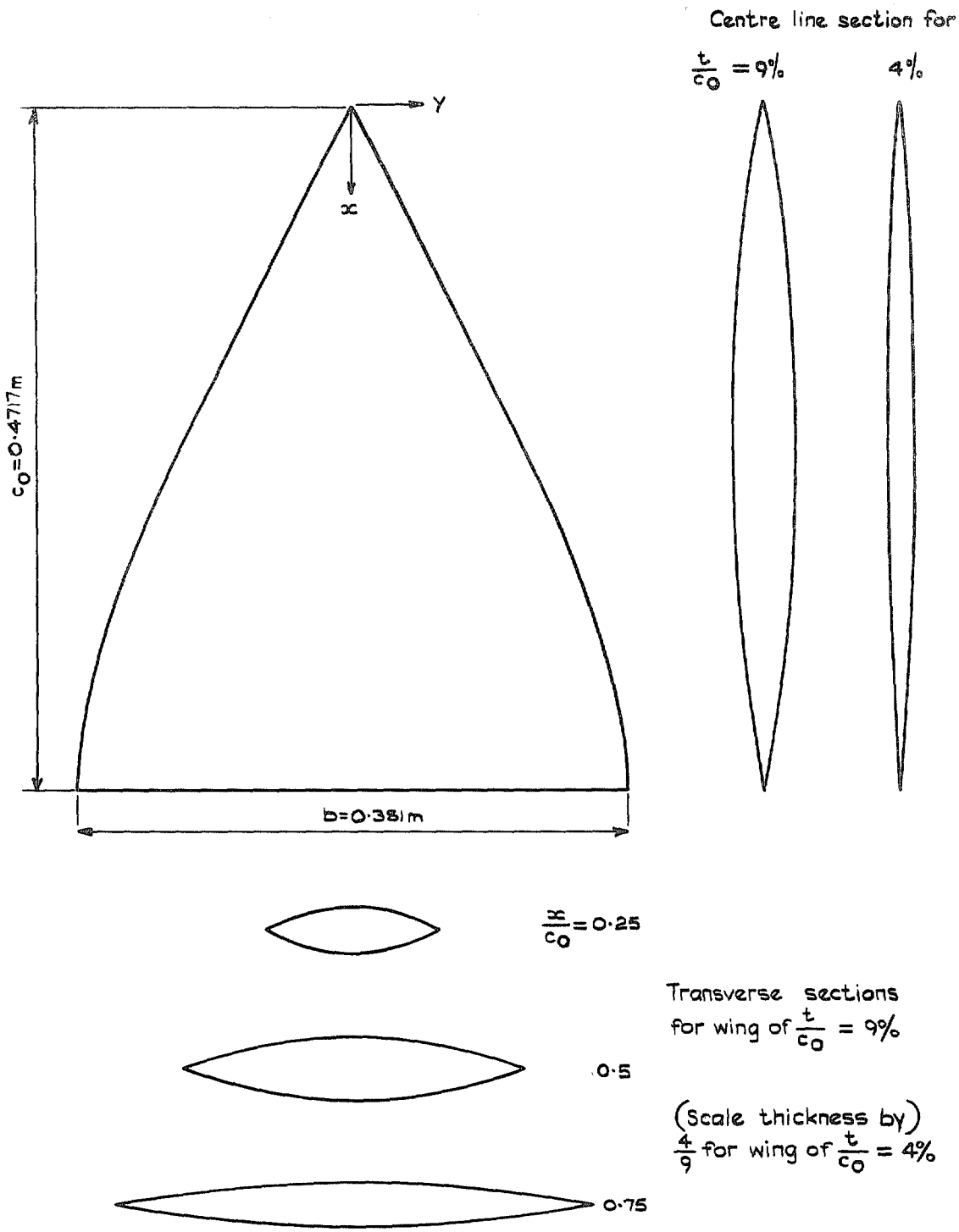

FIG. 1. Planform and sections of wings.

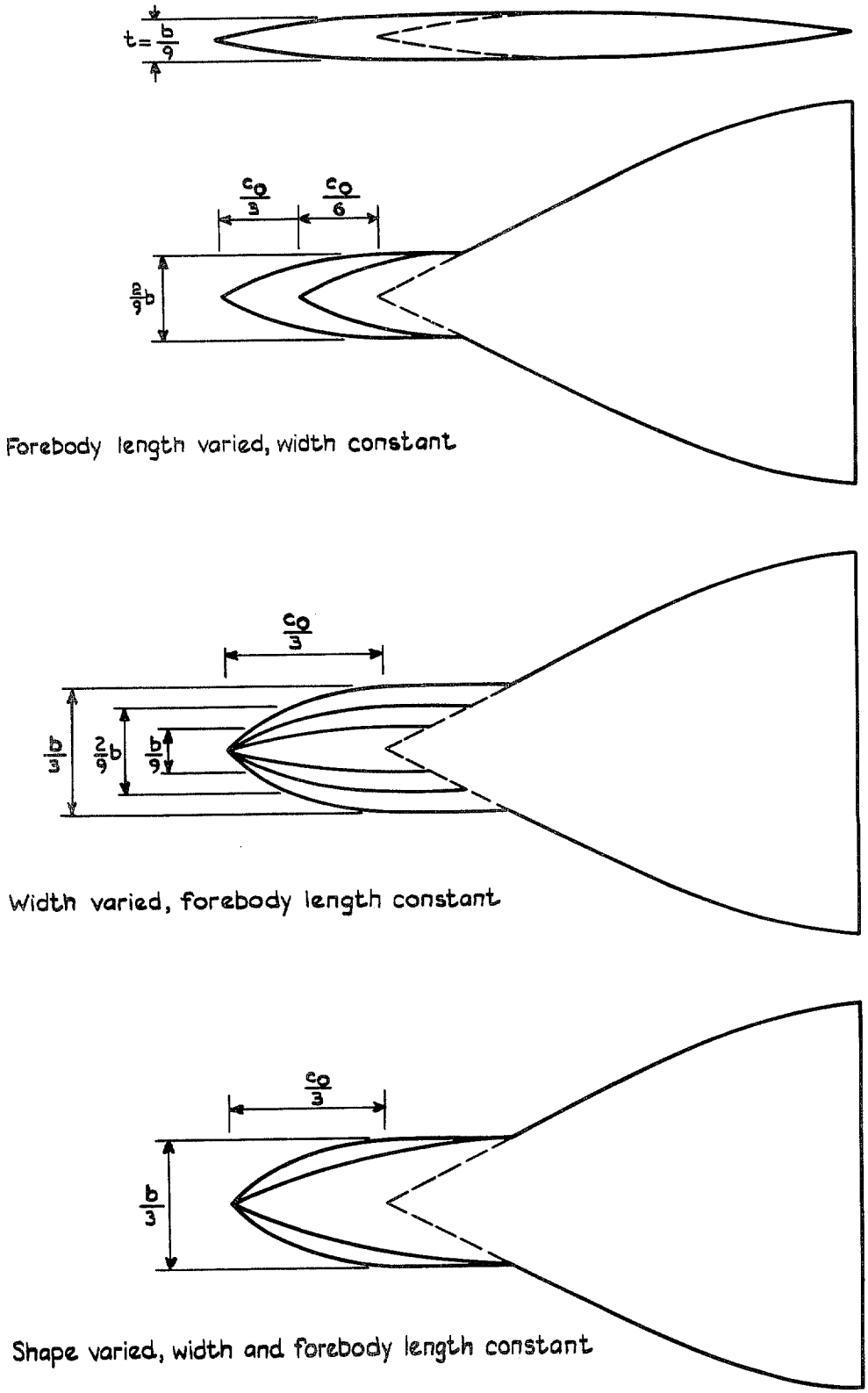

FIG. 2. Planforms of bodies tested on wing of $t/c_0 = 9$ per cent
(Note: Maximum thickness of all bodies = maximum wing thickness).

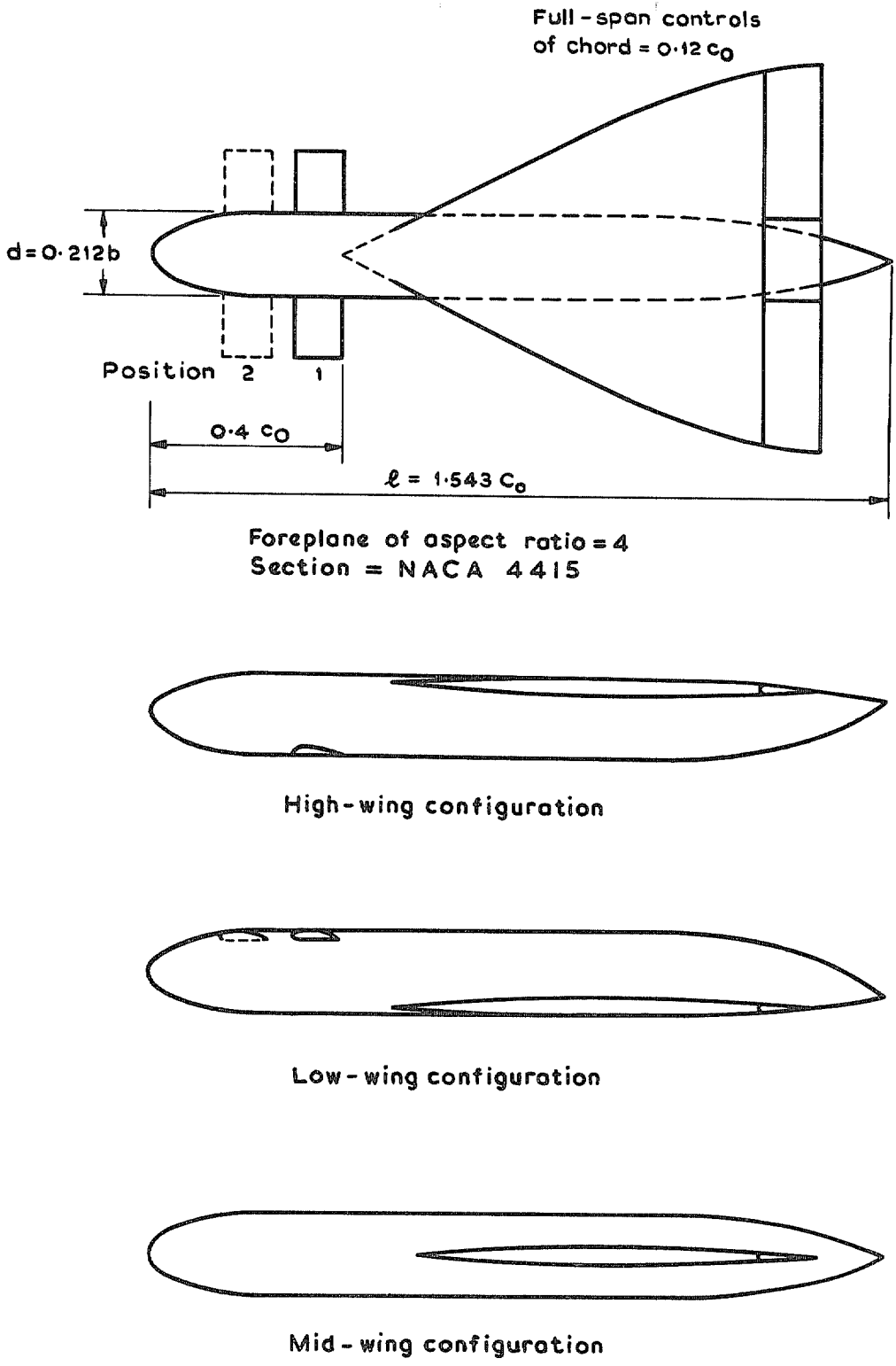

FIG. 3. Layout of models with bodies, wing of $t/c_0 = 4$ per cent and foreplane.

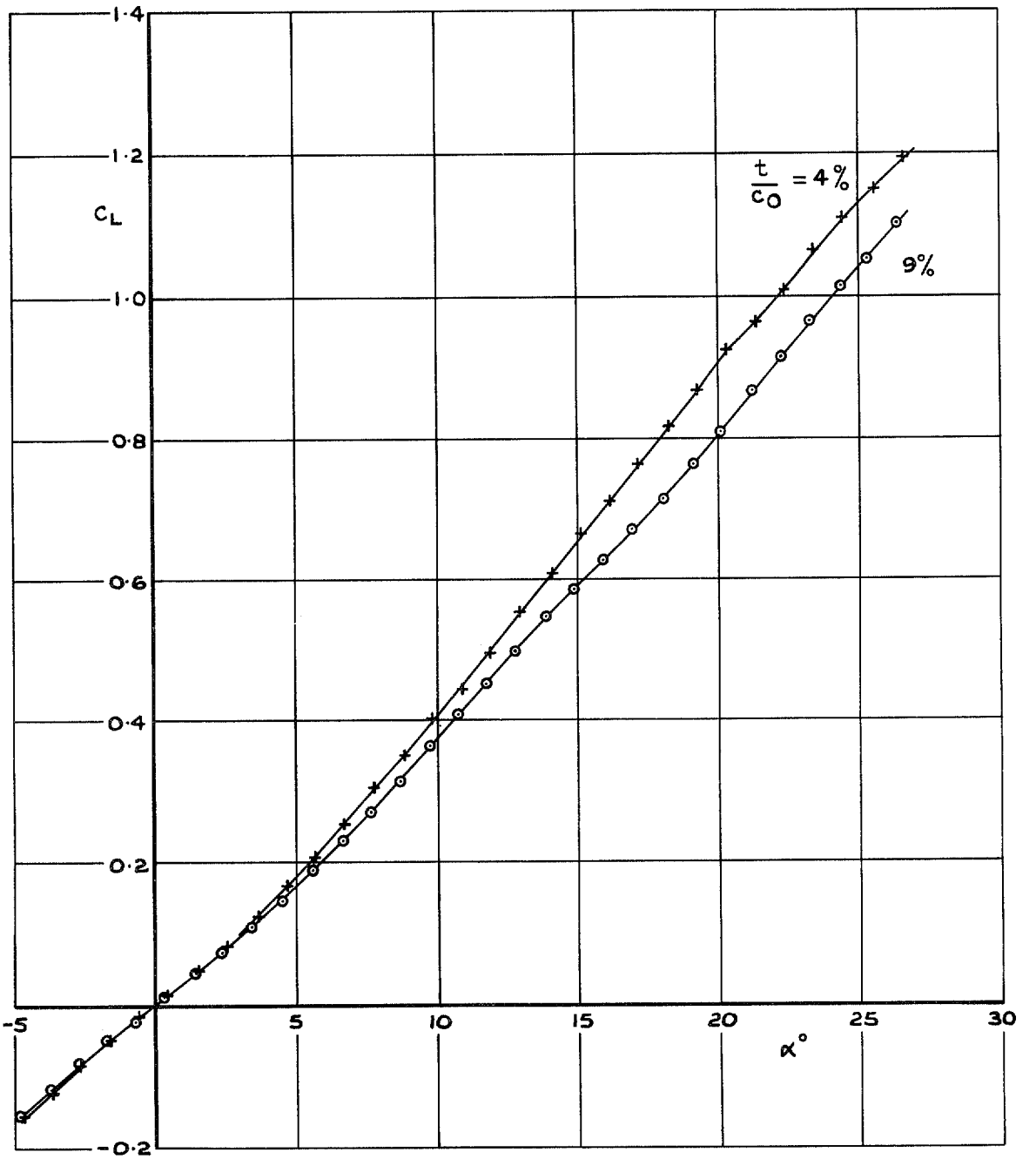

FIG. 4. Effect of wing thickness on lift coefficient.

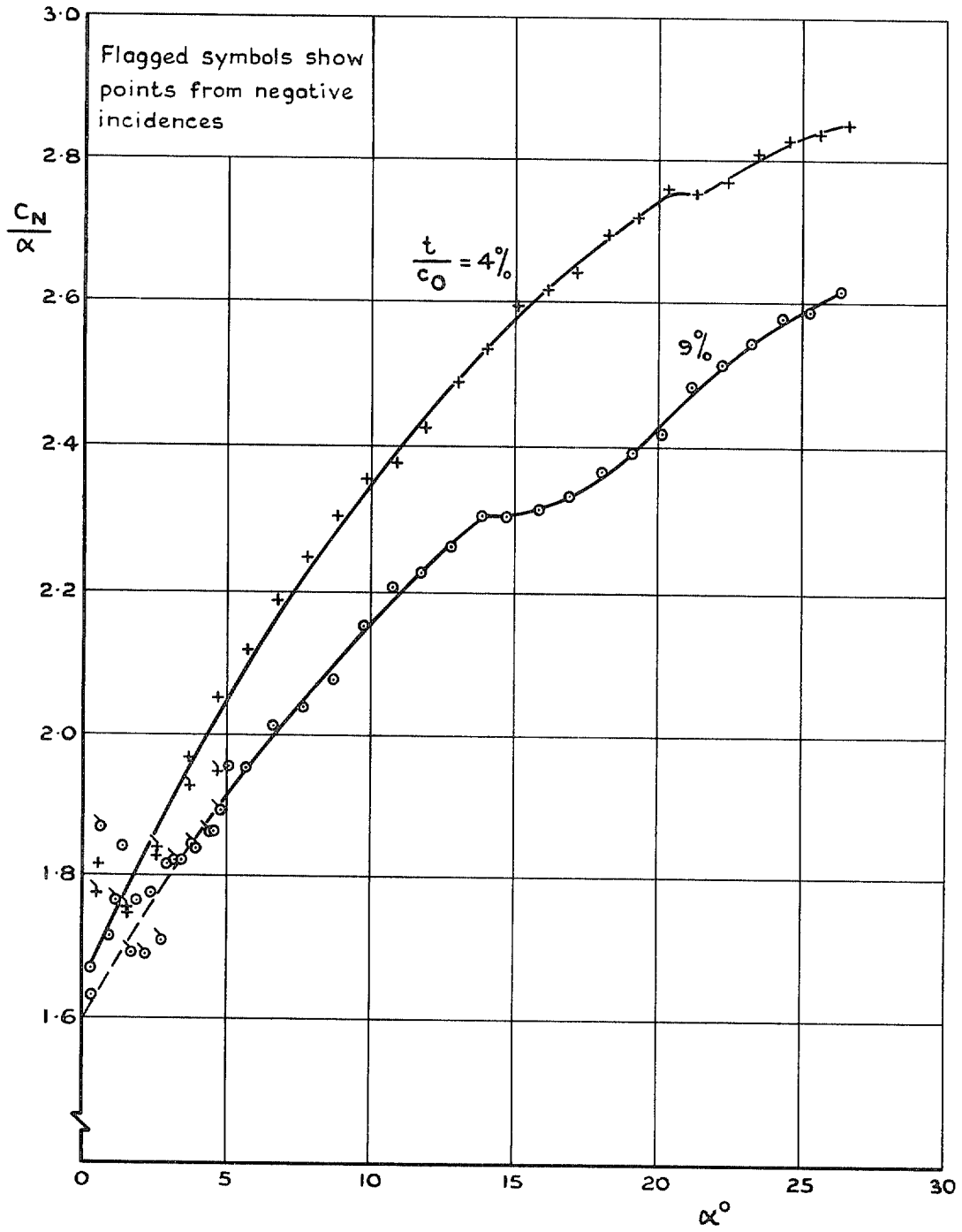

FIG. 5. Effect of wing thickness on C_N/α.

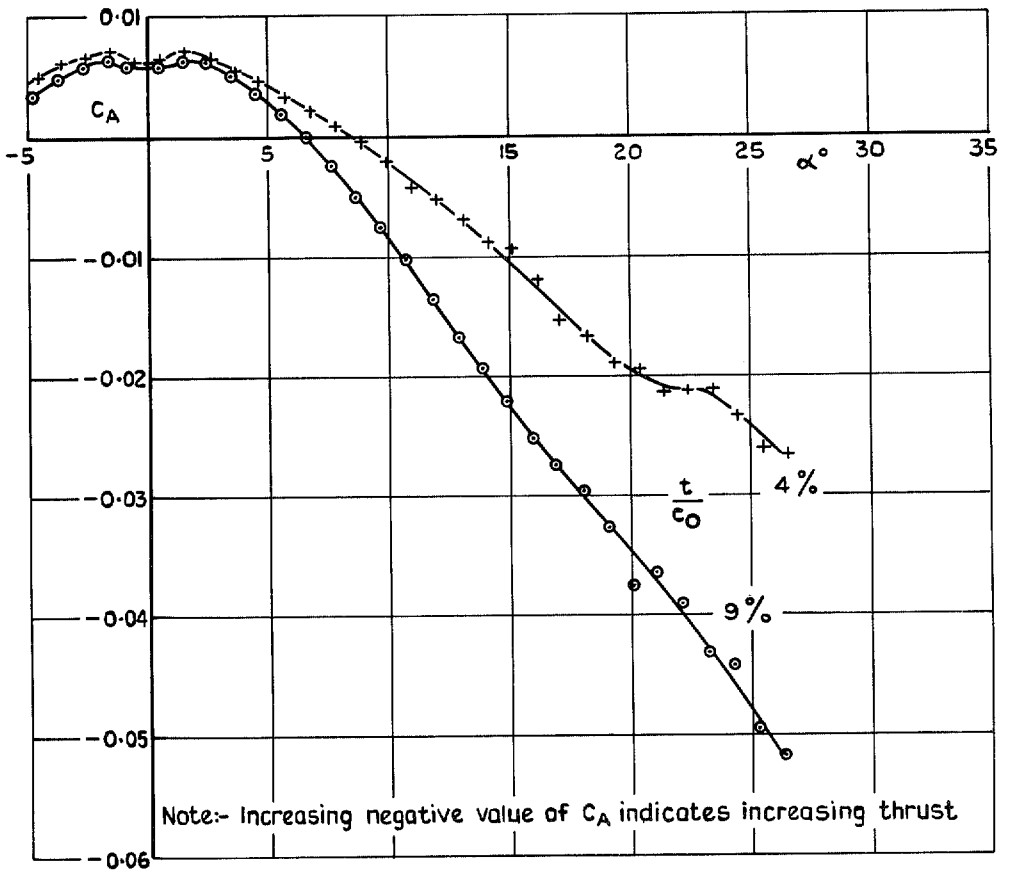

FIG. 6. Effect of wing thickness on axial force coefficient.

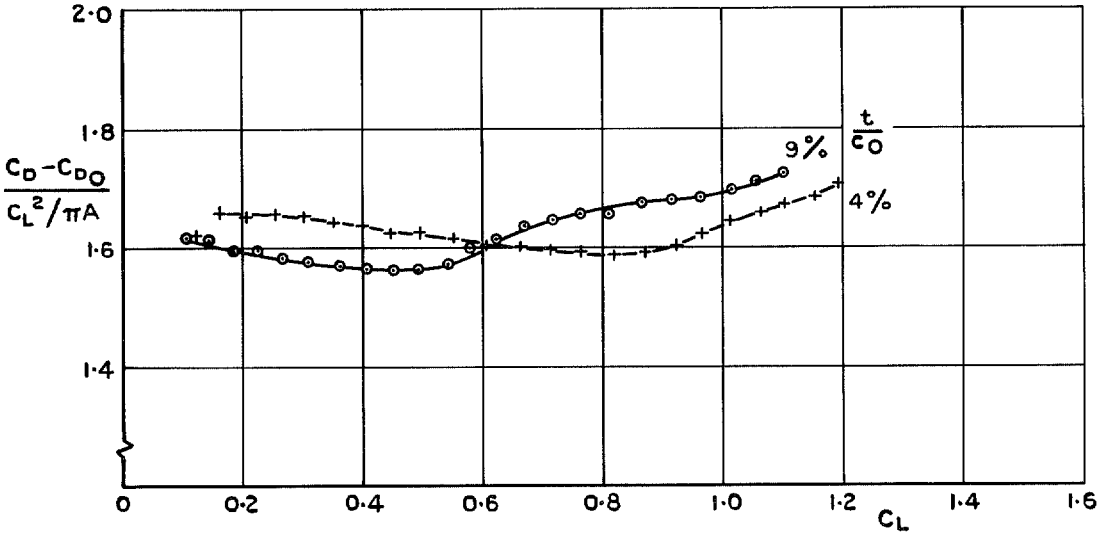

FIG. 7. Effect of wing thickness on lift-dependent drag factor.

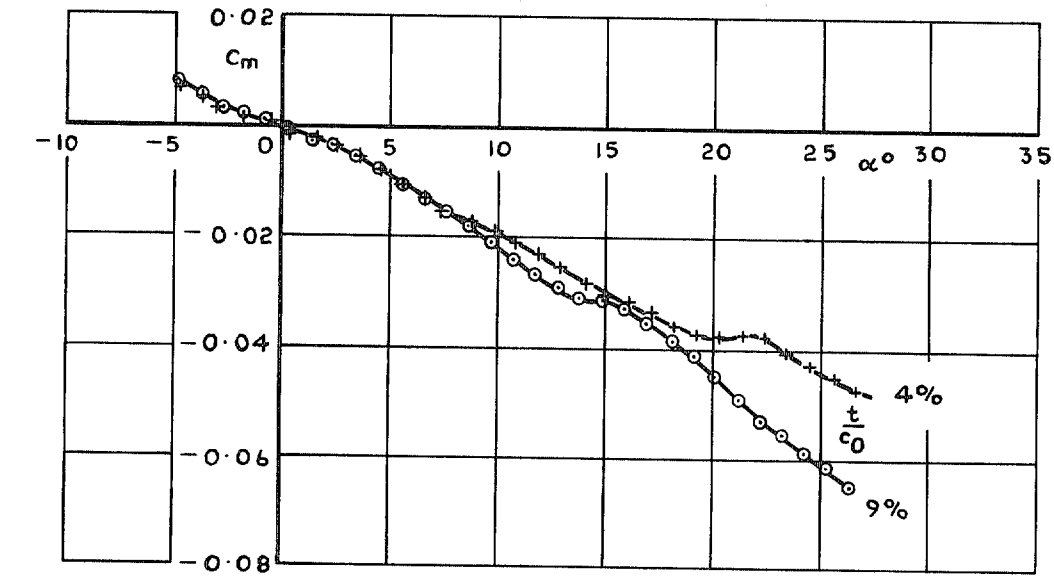

a Cm v α

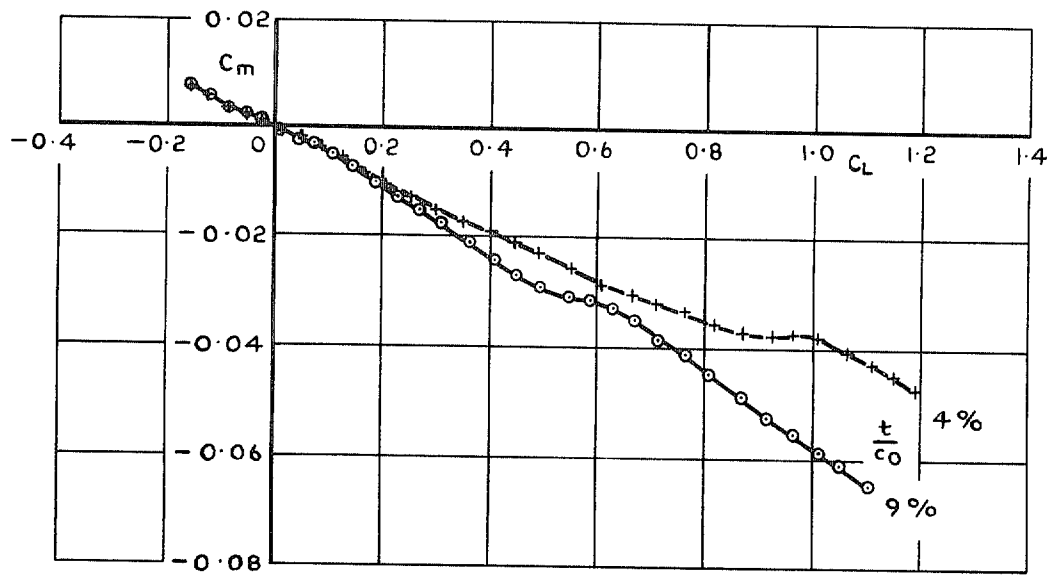

b Cm v CL

FIG. 8a and b. Effect of wing thickness on pitching moment coefficient.

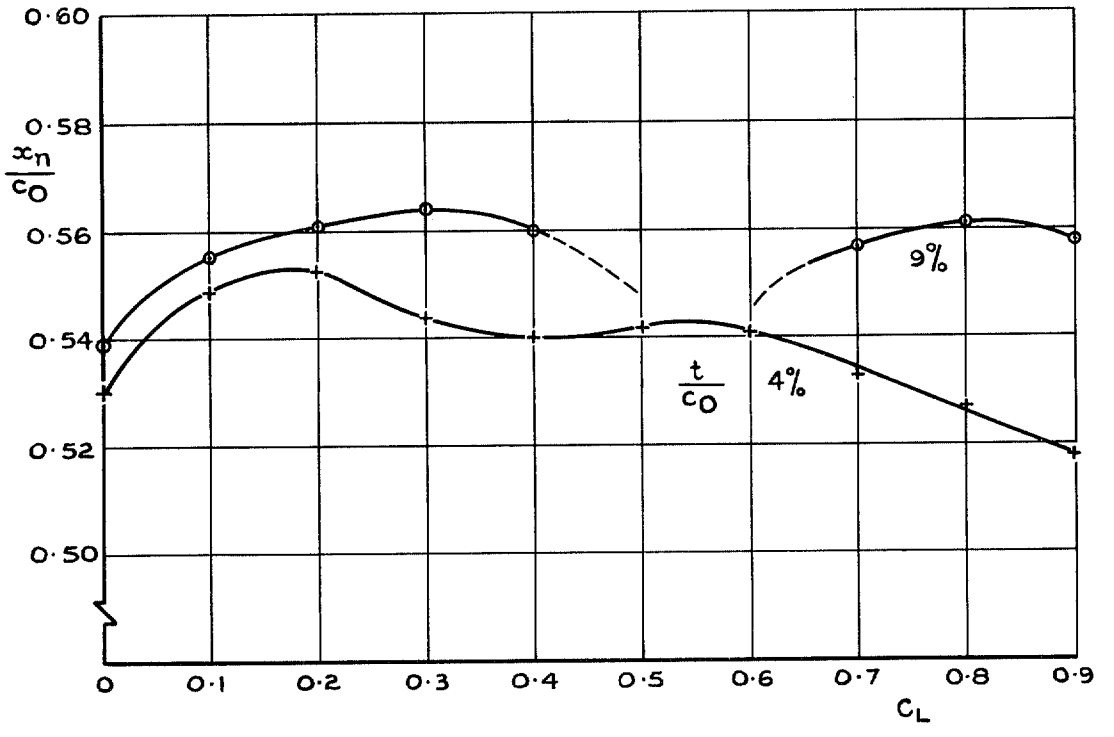

FIG. 9. Effect of wing thickness on aerodynamic centre position.

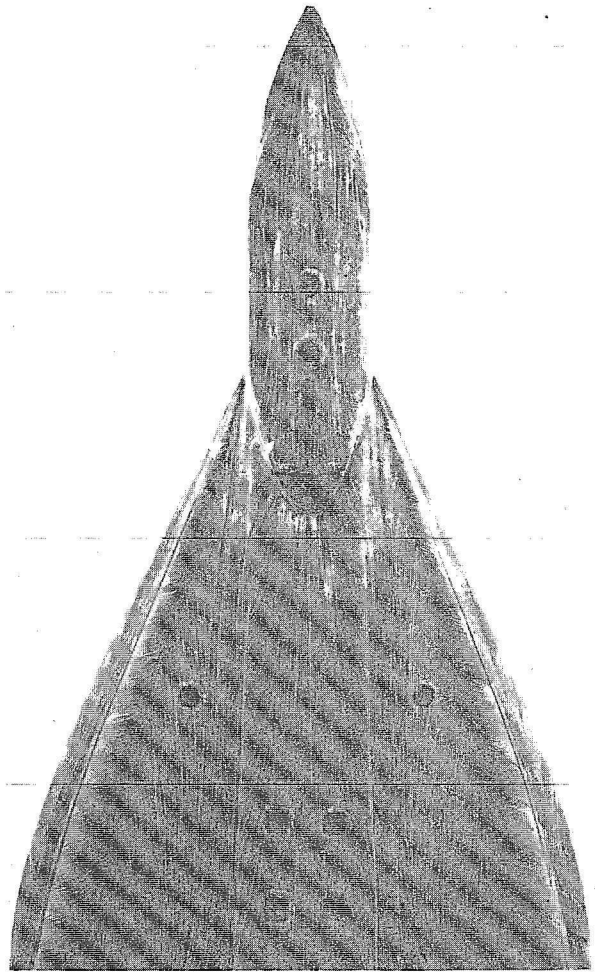

FIG. 10a. $\alpha = 10$ deg, $\frac{w_B}{b} = \frac{2}{9}$, $\frac{f_B}{c_0} = \frac{1}{3}$.

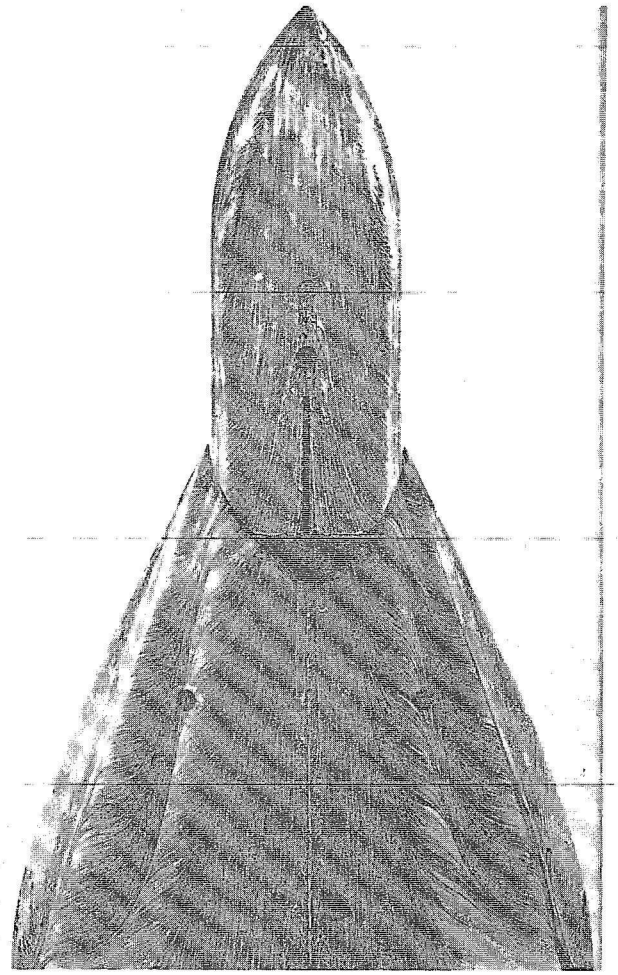

FIG. 10b. $\alpha = 15$ deg, $\frac{w_B}{b} = \frac{1}{3}$, $\frac{f_B}{c_0} = \frac{1}{3}$.

FIG. 10. Surface flow patterns. Tunnel speed = 30·4 m s.

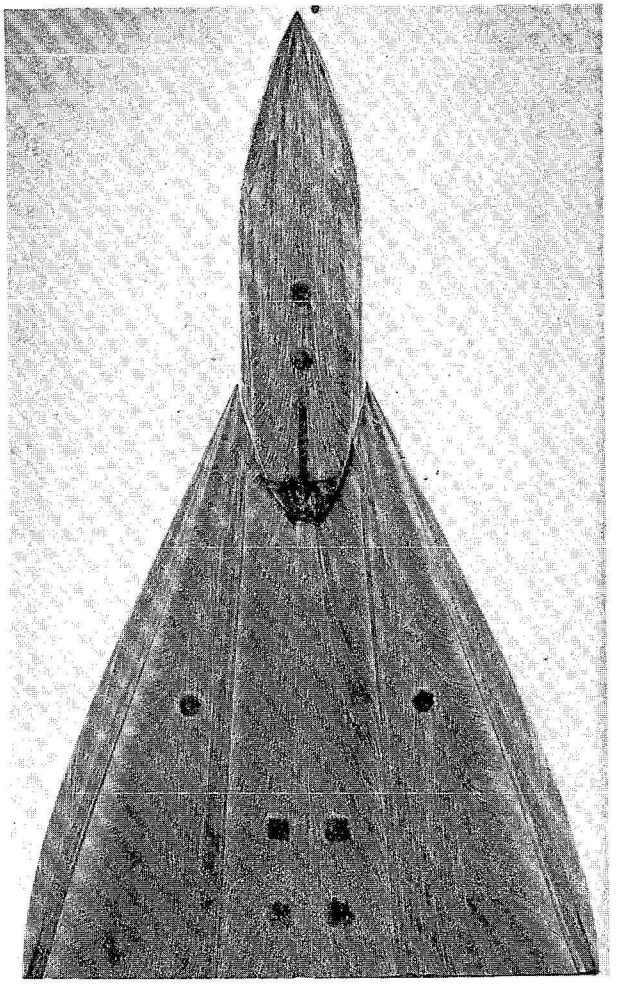

FIG. 10c. $\alpha = 15$ deg, $\frac{w_B}{b} = \frac{2}{9}$, $\frac{f_B}{c_0} = \frac{1}{3}$.

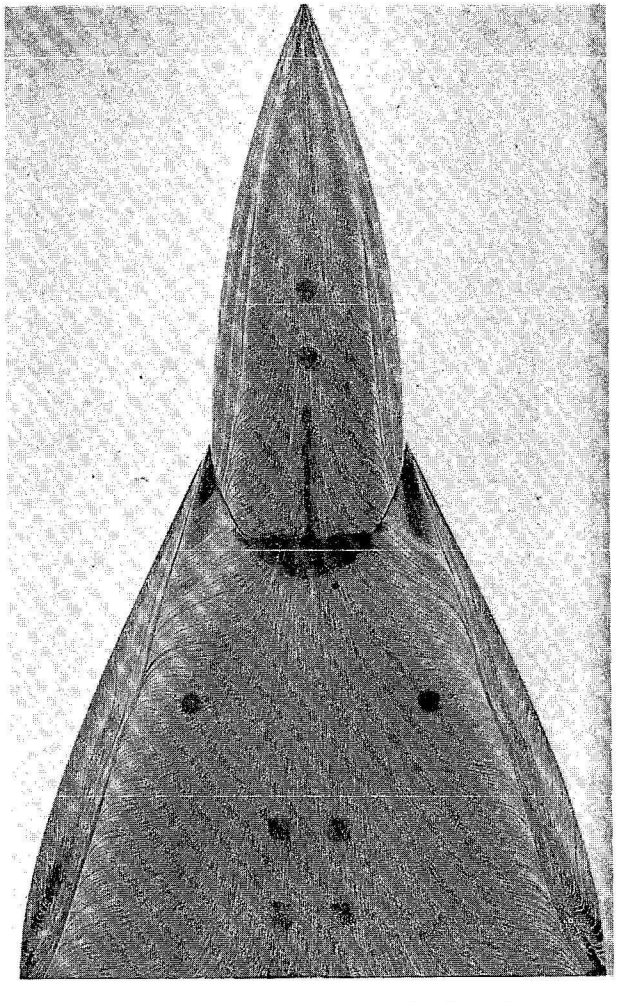

FIG. 10d. $\alpha = 25$ deg, $\frac{w_B}{b} = \frac{1}{3}$, $\frac{f_B}{c_0} = \frac{1}{3}$.

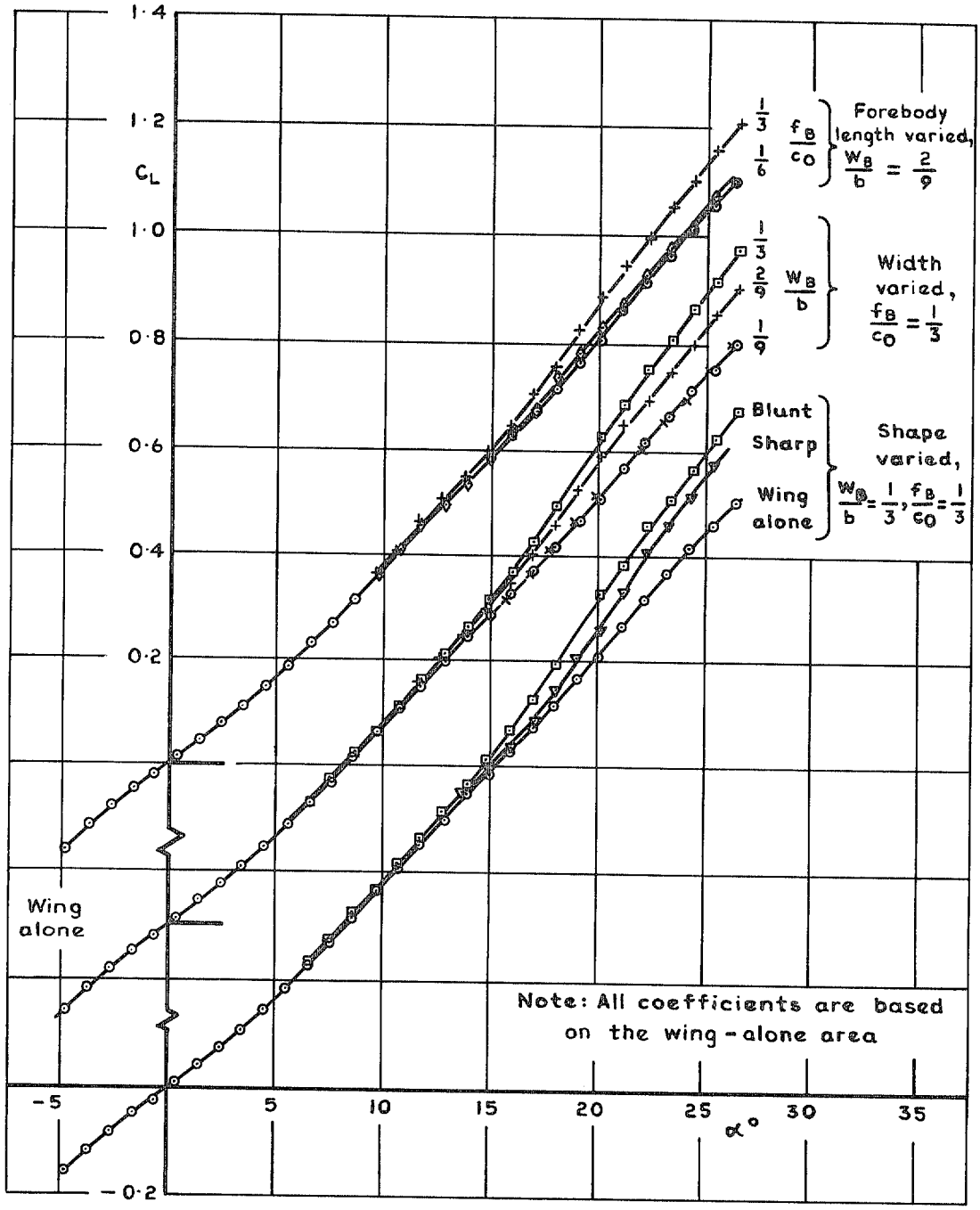

FIG. 11. Effect of varying body parameters on lift coefficient, wing $t/c_0 = 9$ per cent.

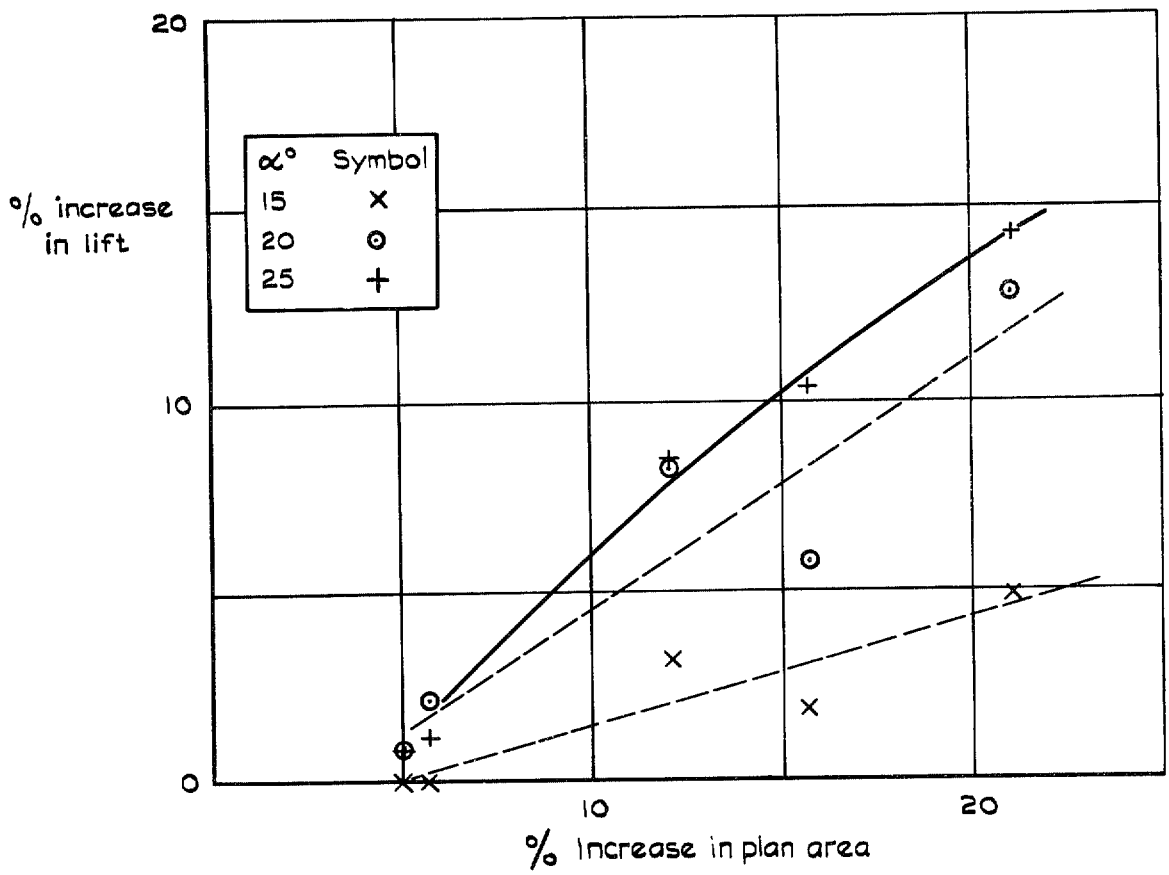

FIG. 12. Increase in lift at constant angle of incidence when bodies added, wing $t/c_0 = 9$ per cent.

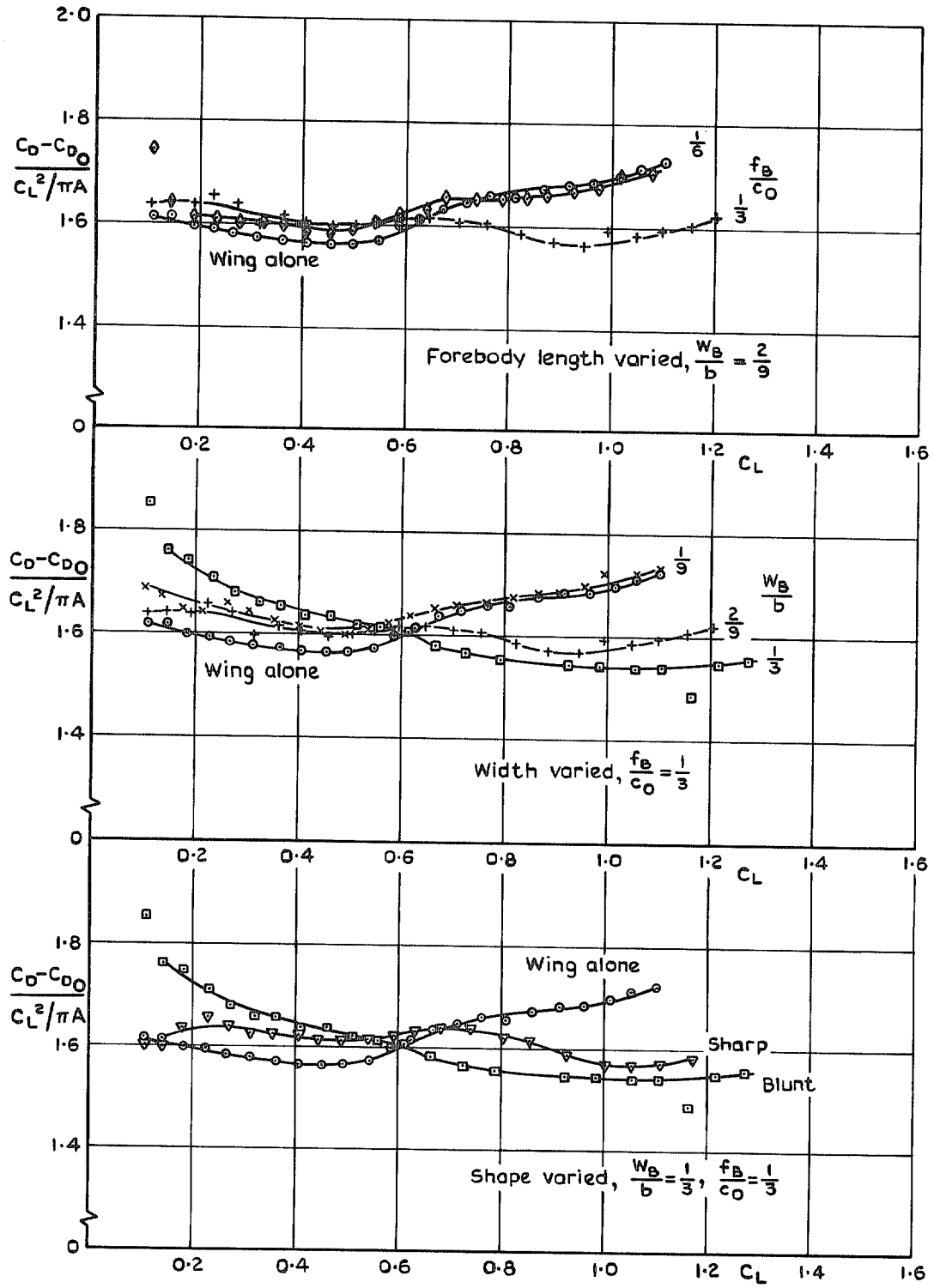

FIG. 13. Effect of varying body parameters on lift-dependent drag factor, wing $t/c_0 = 9$ per cent.

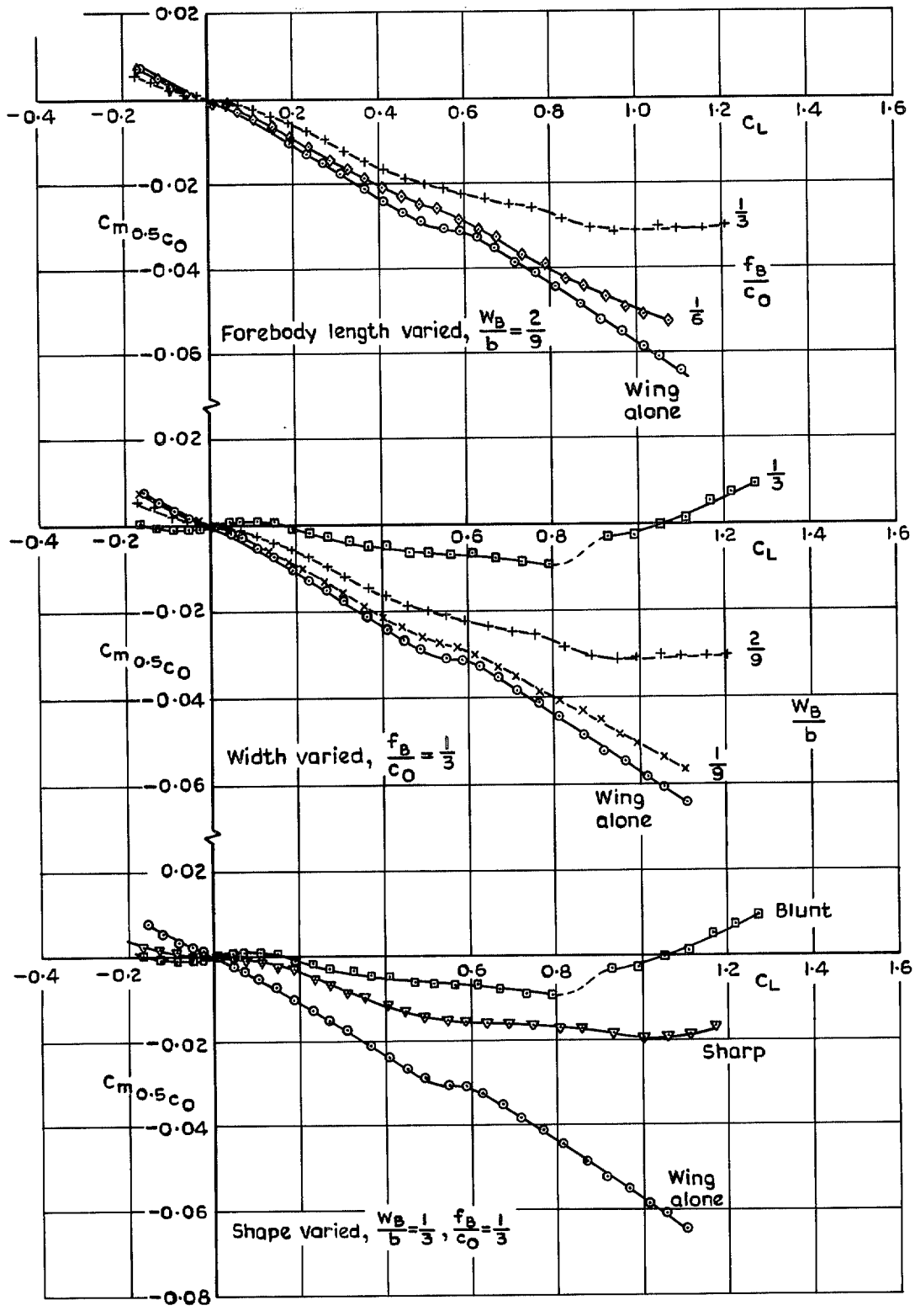

FIG. 14. Effect of varying body parameters on pitching moment coefficient, wing $t/c_0 = 9$ per cent.

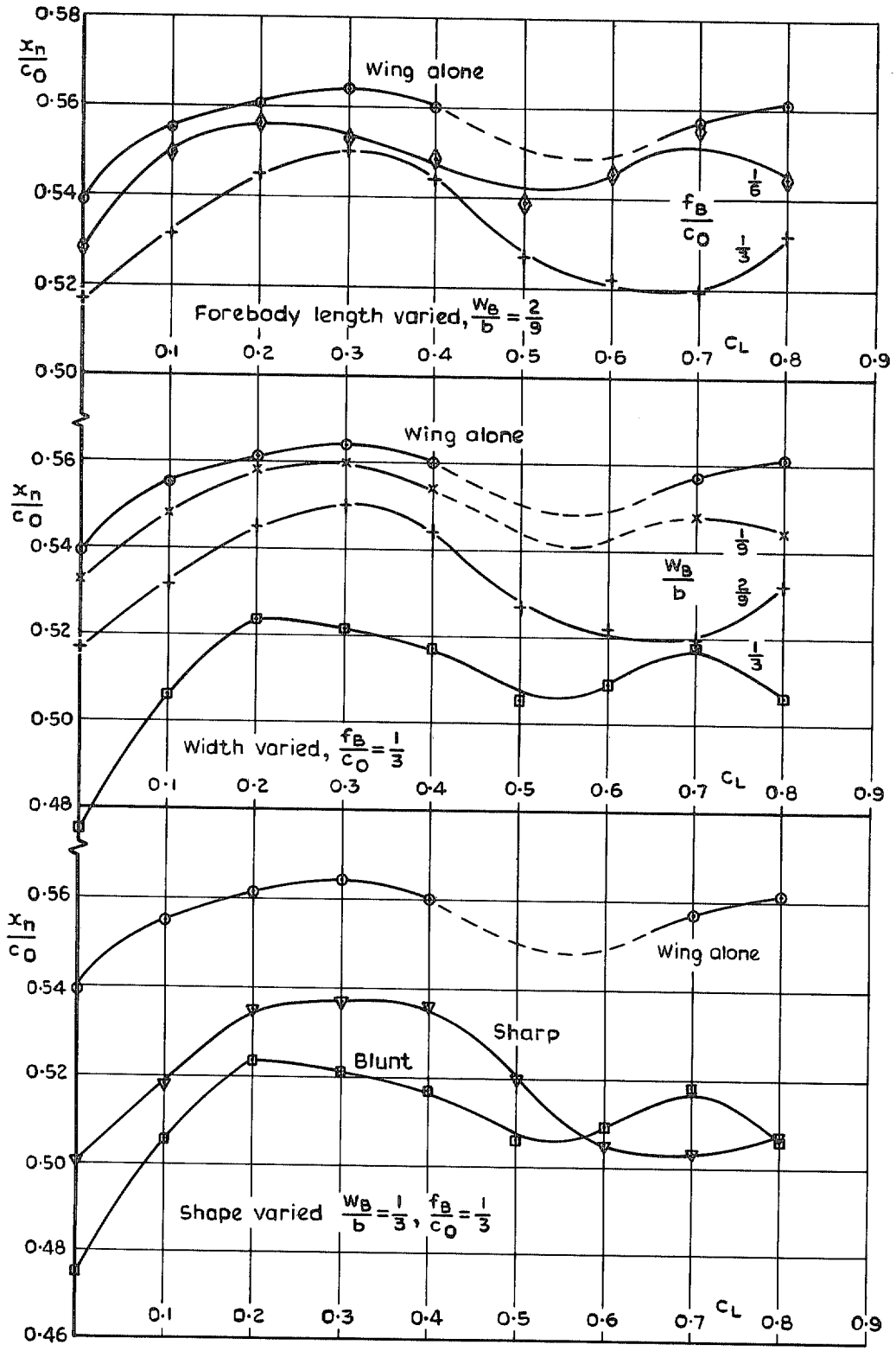

FIG. 15. Effect of varying body parameters on aerodynamic centre position, wing $t/c_0 = 9$ per cent.

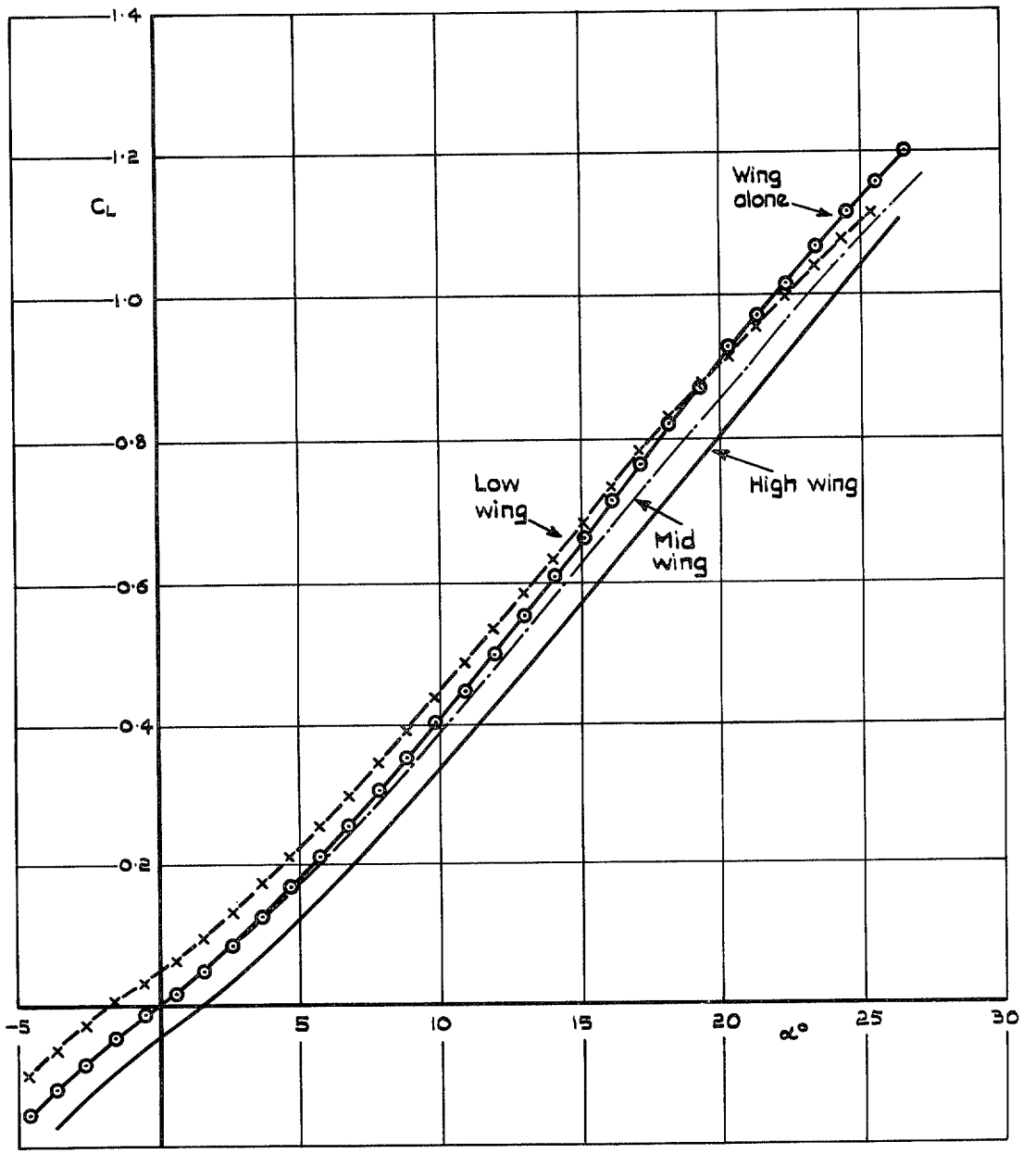

FIG. 16. Lift coefficient of 4 per cent t/c_0 wing with and without a body, $\eta = 0°$.

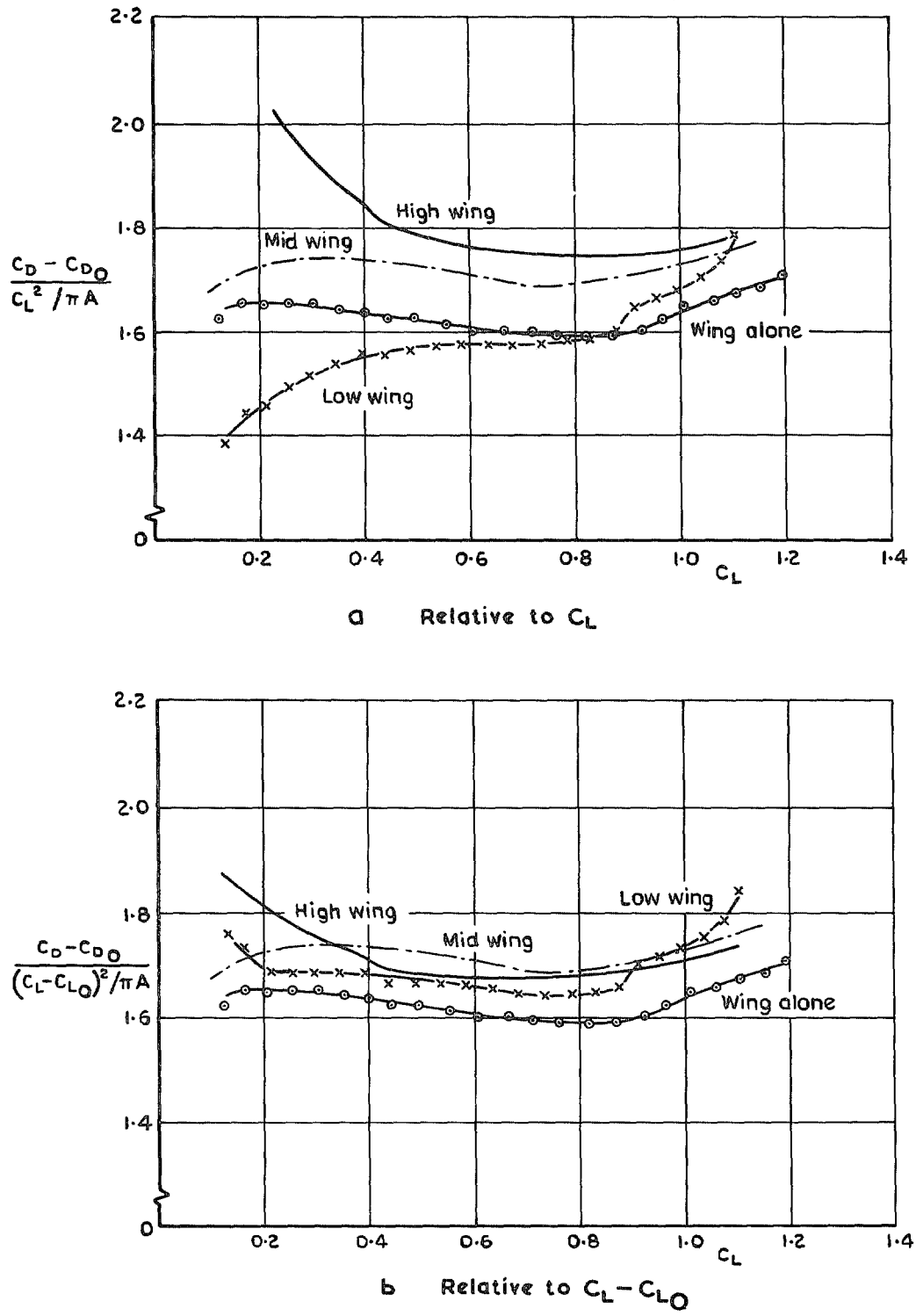

FIG. 17a & b. Lift-dependent drag factor for 4 per cent t/c_0 wing with and without a body, $\eta = 0°$.

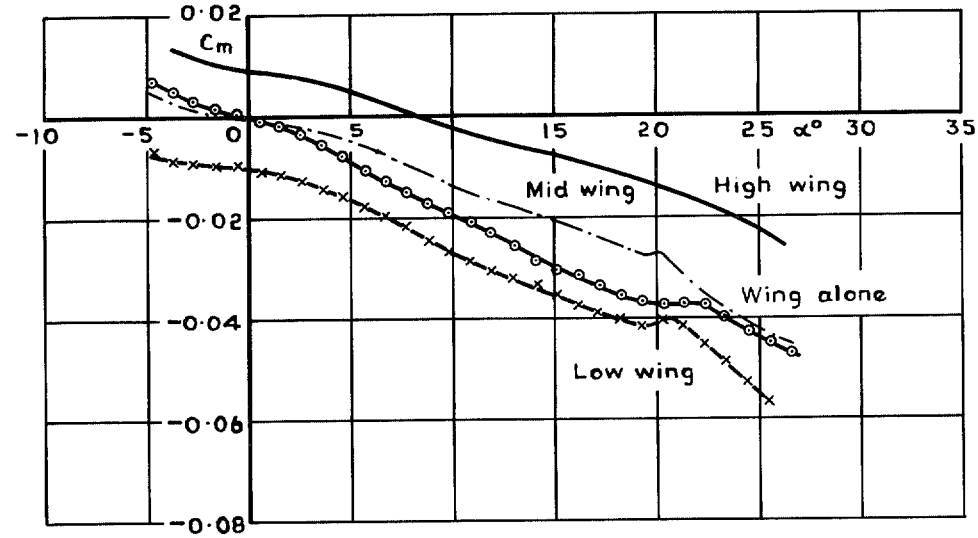

a Cm v α

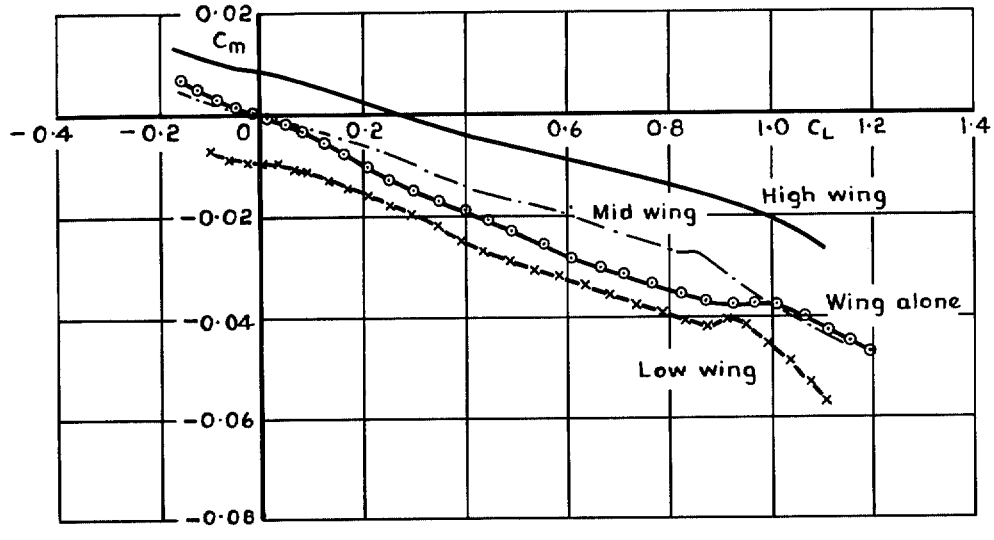

b Cm v CL

FIG. 18a & b. Pitching moment coefficient of 4 per cent t/c_0 wing with and without a body, $\eta = 0°$.

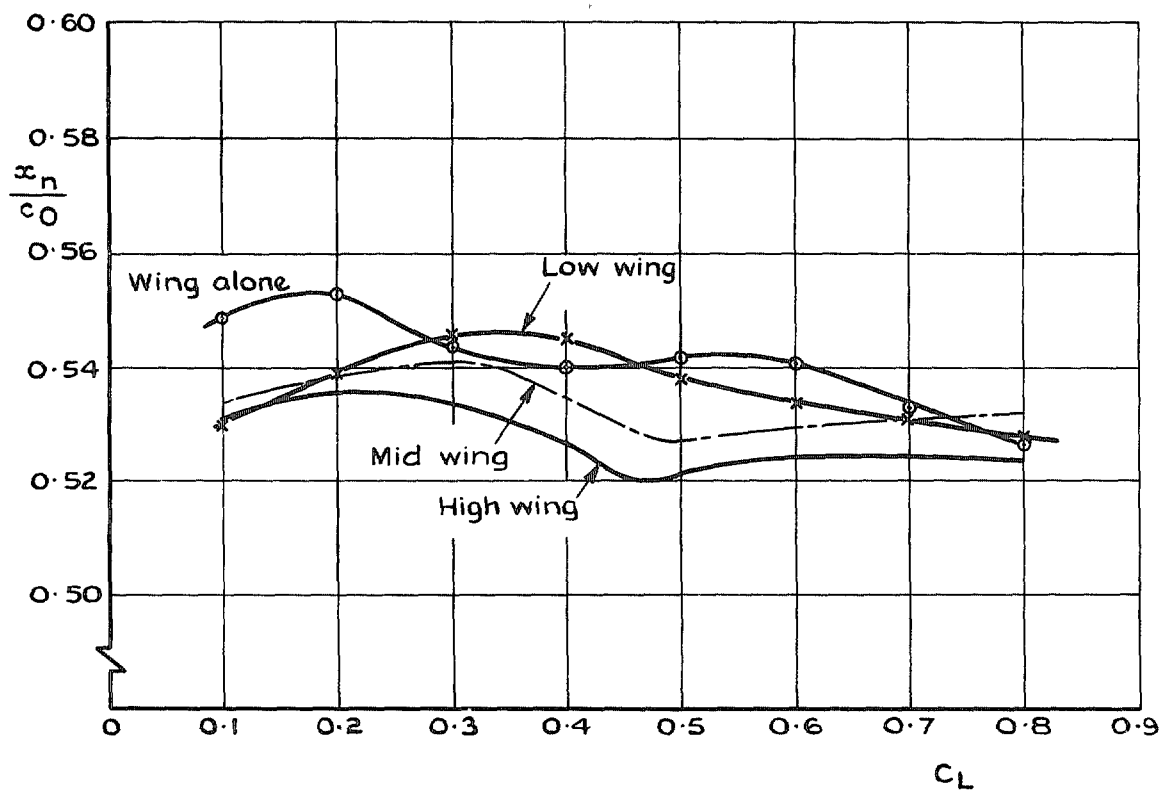

FIG. 19. Aerodynamic centre position for 4 per cent t/c_0 wing with and without a body, $\eta = 0°$.

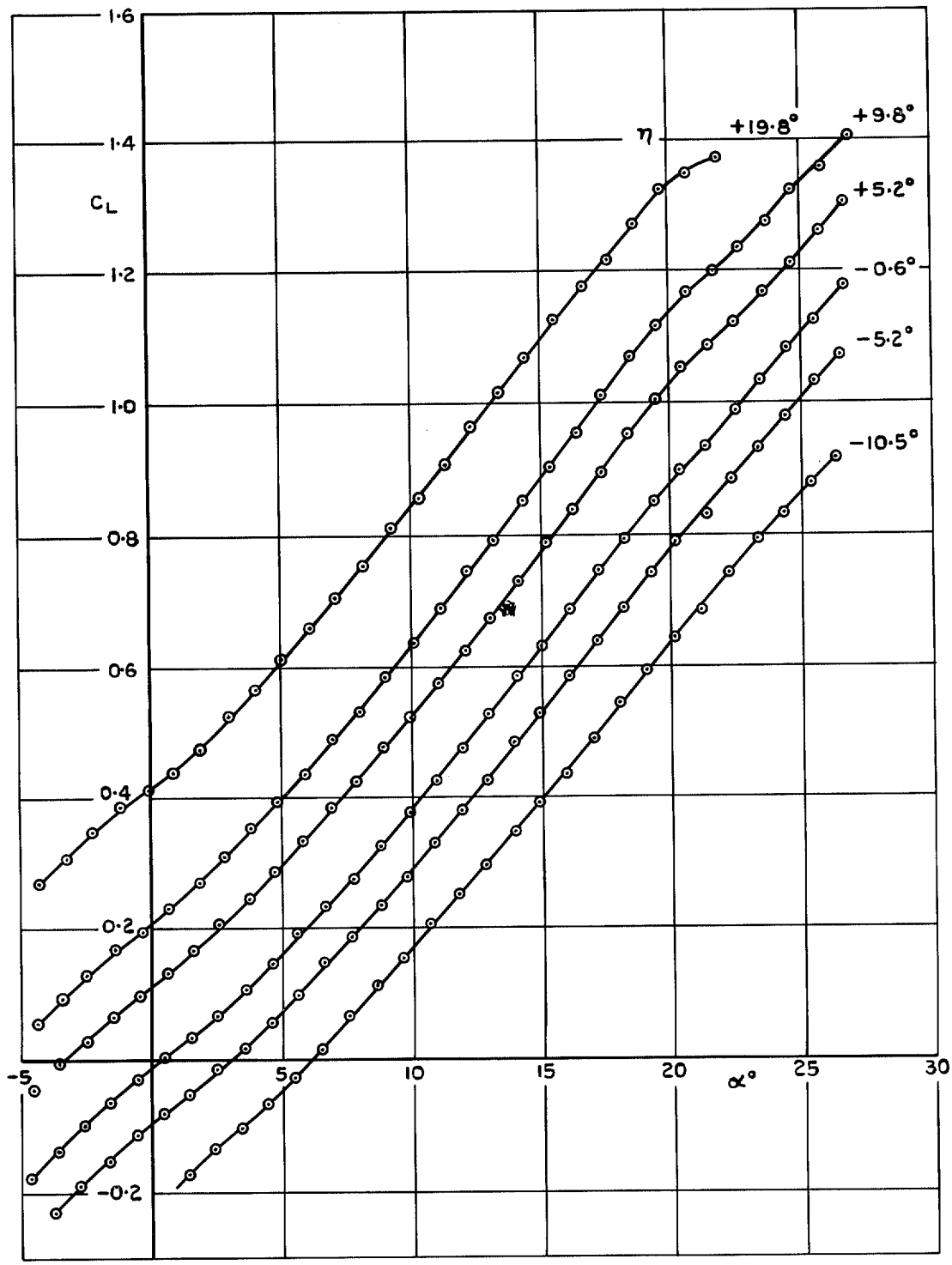

FIG. 20. Lift coefficient of 4 per cent t/c_0 wing with trailing-edge controls deflected.

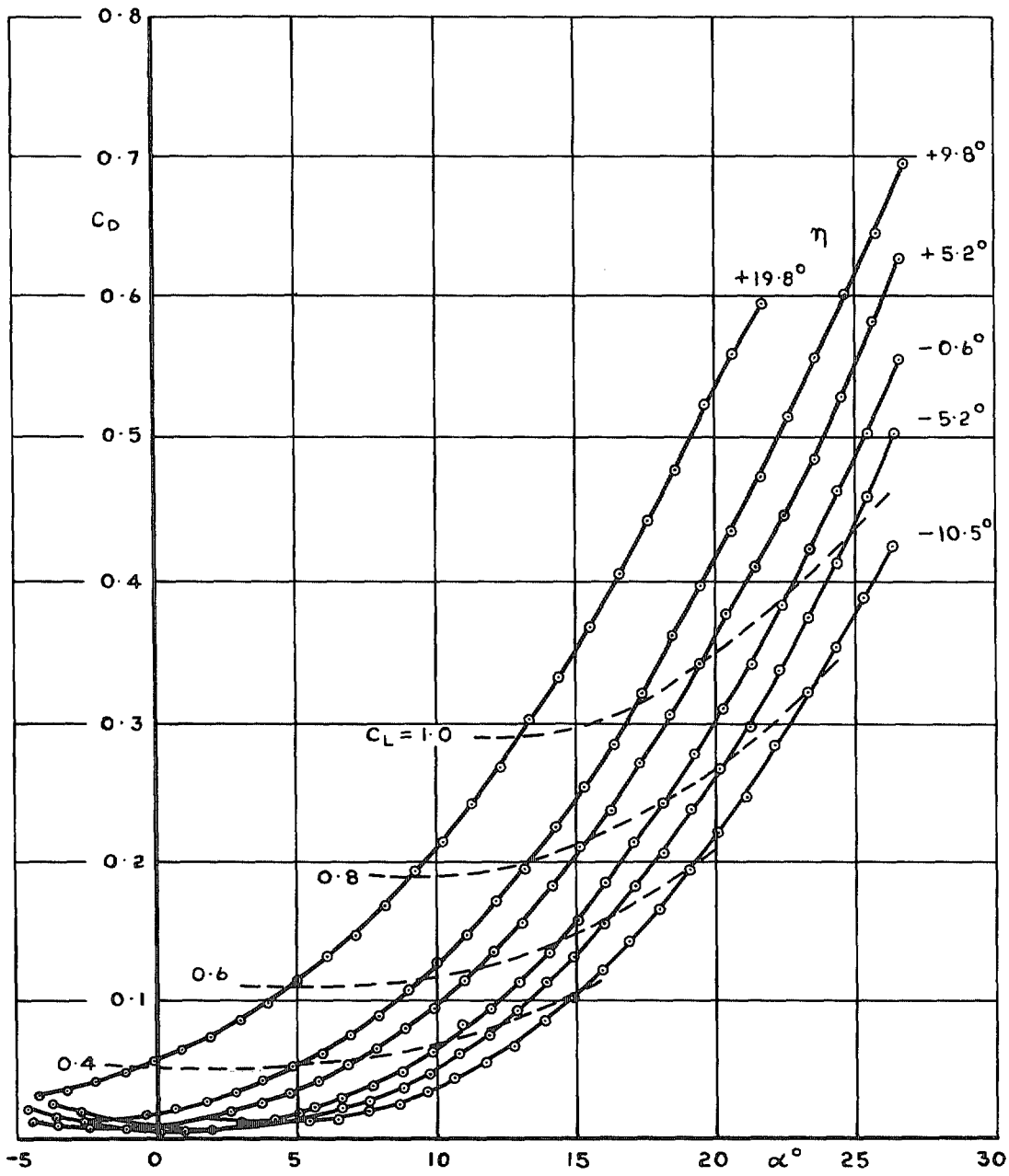

FIG. 21. Drag coefficient of 4 per cent t/c_0 wing with trailing-edge controls deflected.

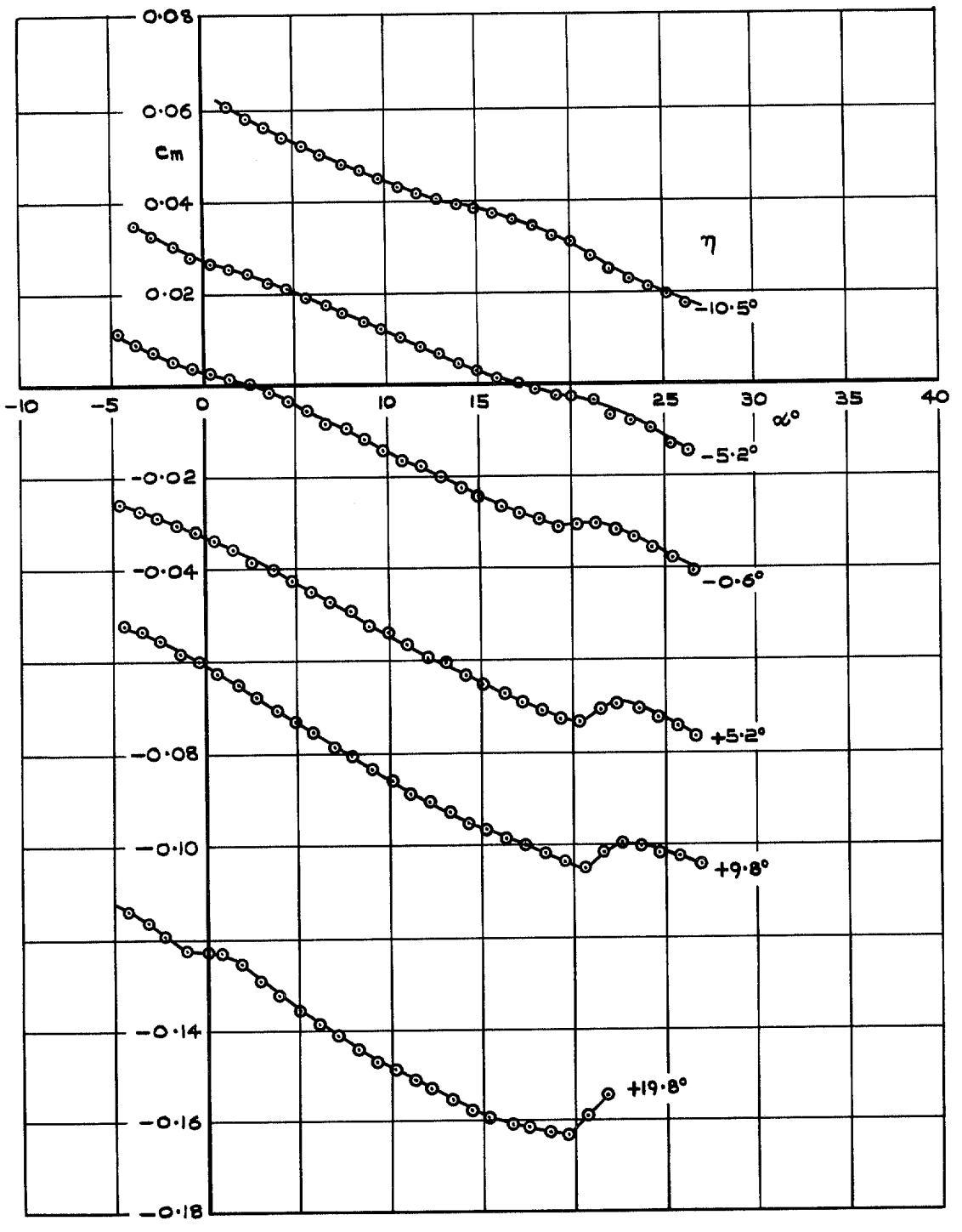

FIG. 22. Pitching moment coefficient of 4 per cent t/c_0 wing with trailing-edge controls deflected.

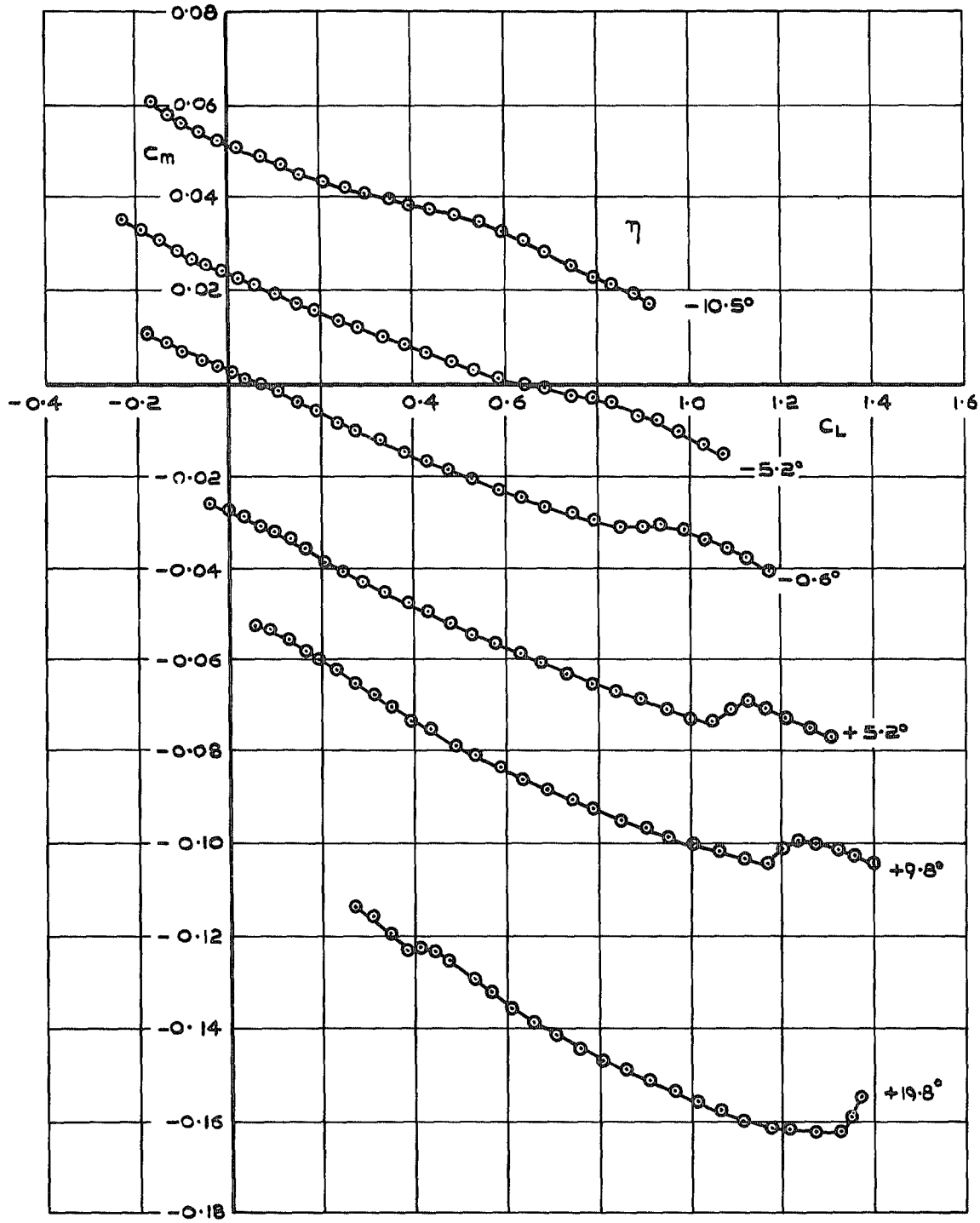

FIG. 23. Pitching moment coefficient v lift coefficient for 4 per cent t/c_0 wing with trailing-edge controls deflected.

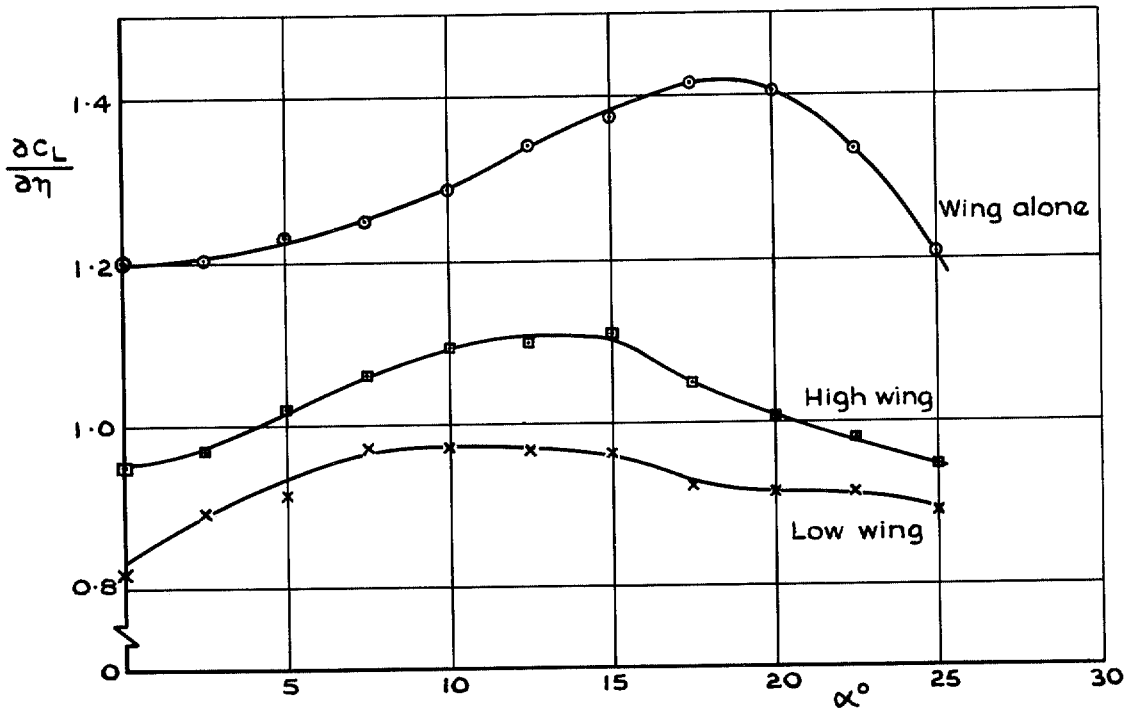

a Lift

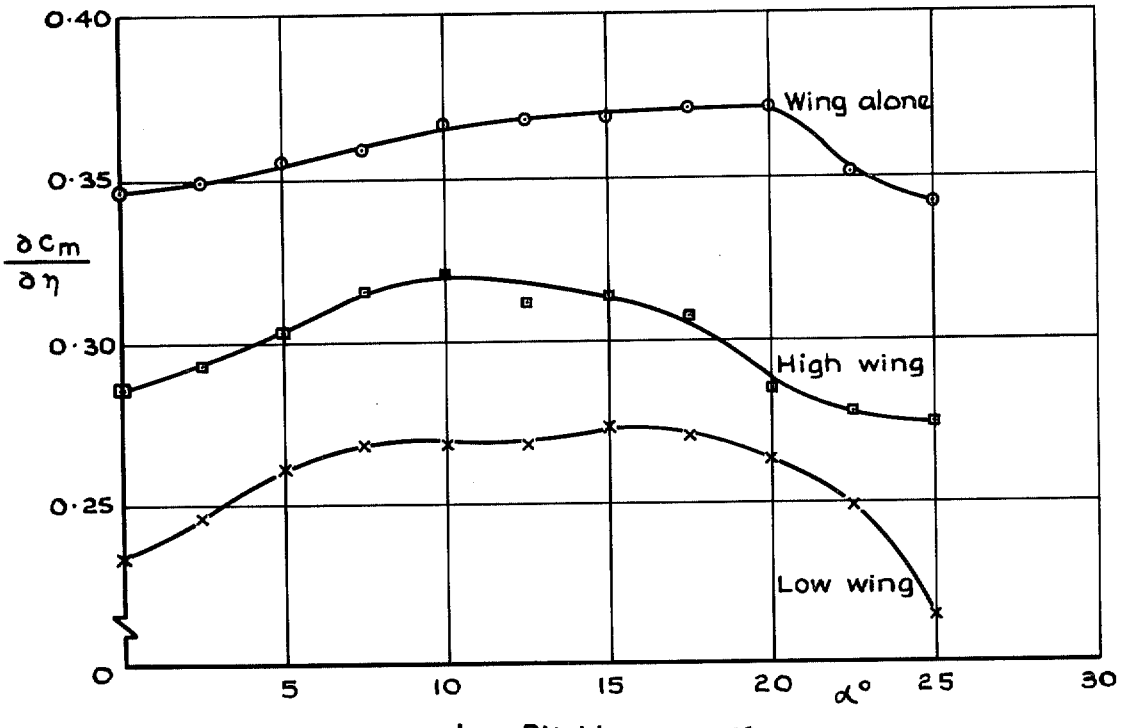

b Pitching moment

FIG. 24a & b. Control powers for 4 per cent t/c_0 wing.

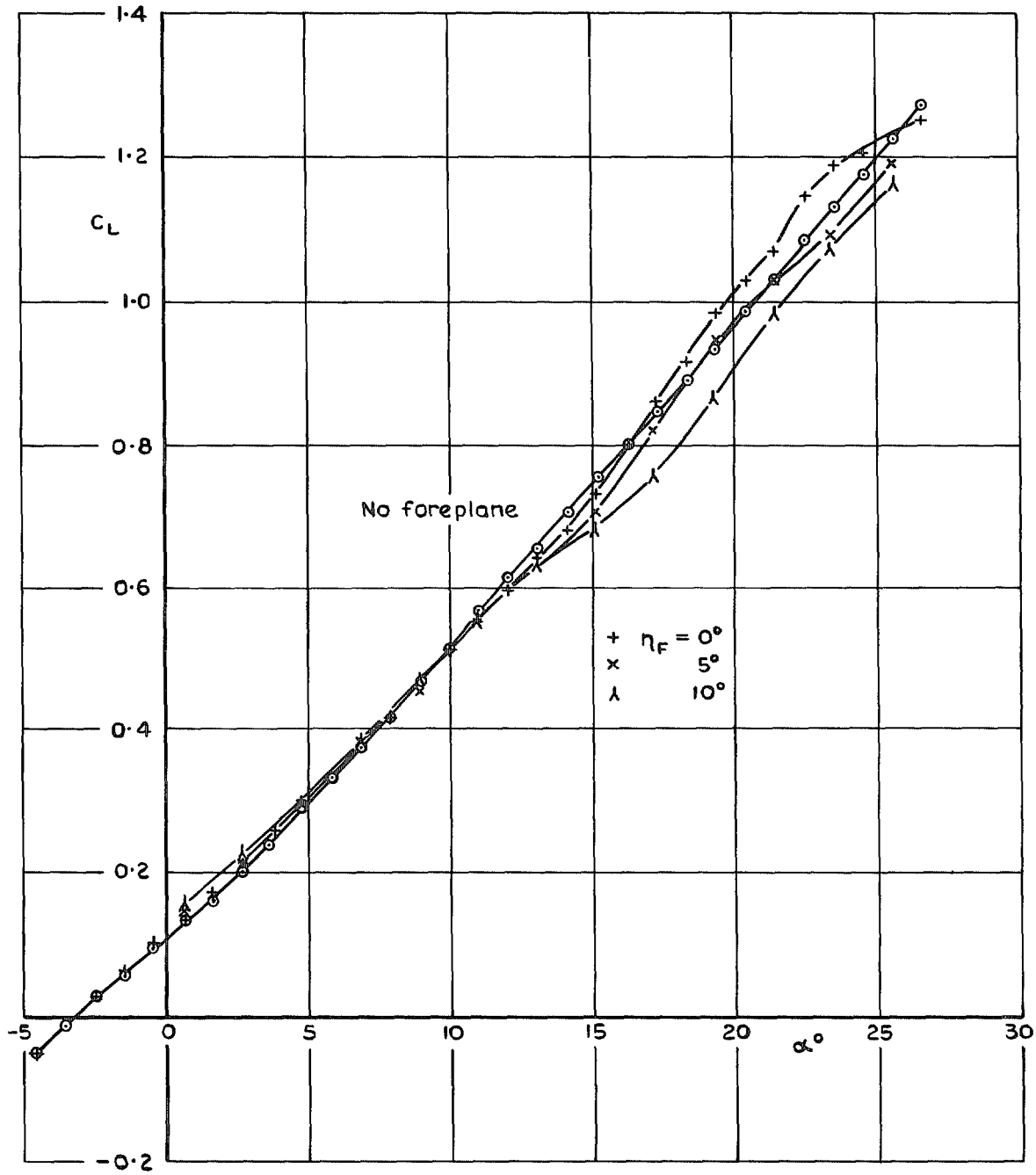

FIG. 25. Lift coefficient for high-wing configuration with low foreplane, trailing-edge controls deflected, $\eta = 10°$.

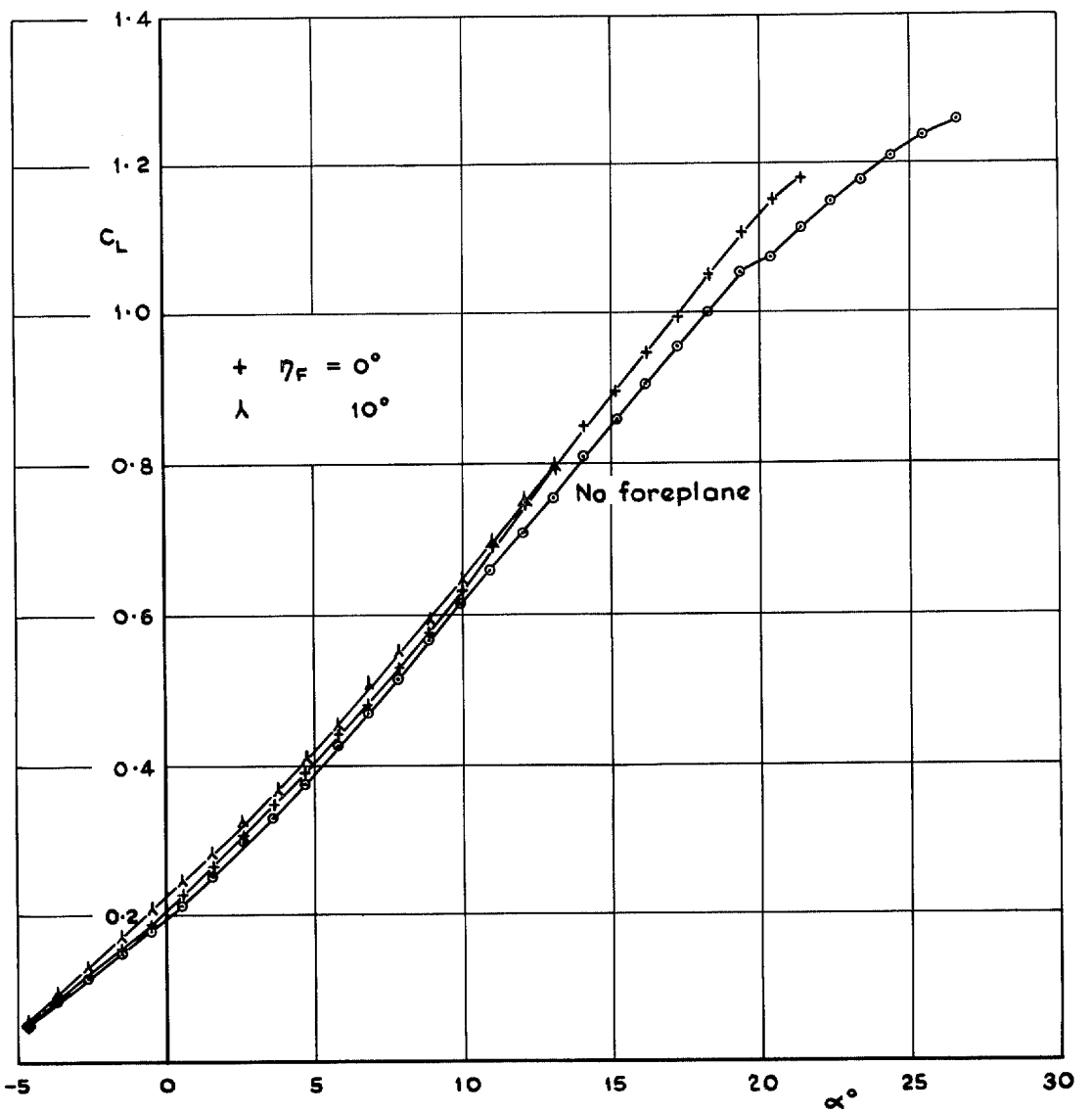

FIG. 26. Lift coefficient for low-wing configuration with high foreplane, trailing-edge controls deflected, $\eta = 10°$.

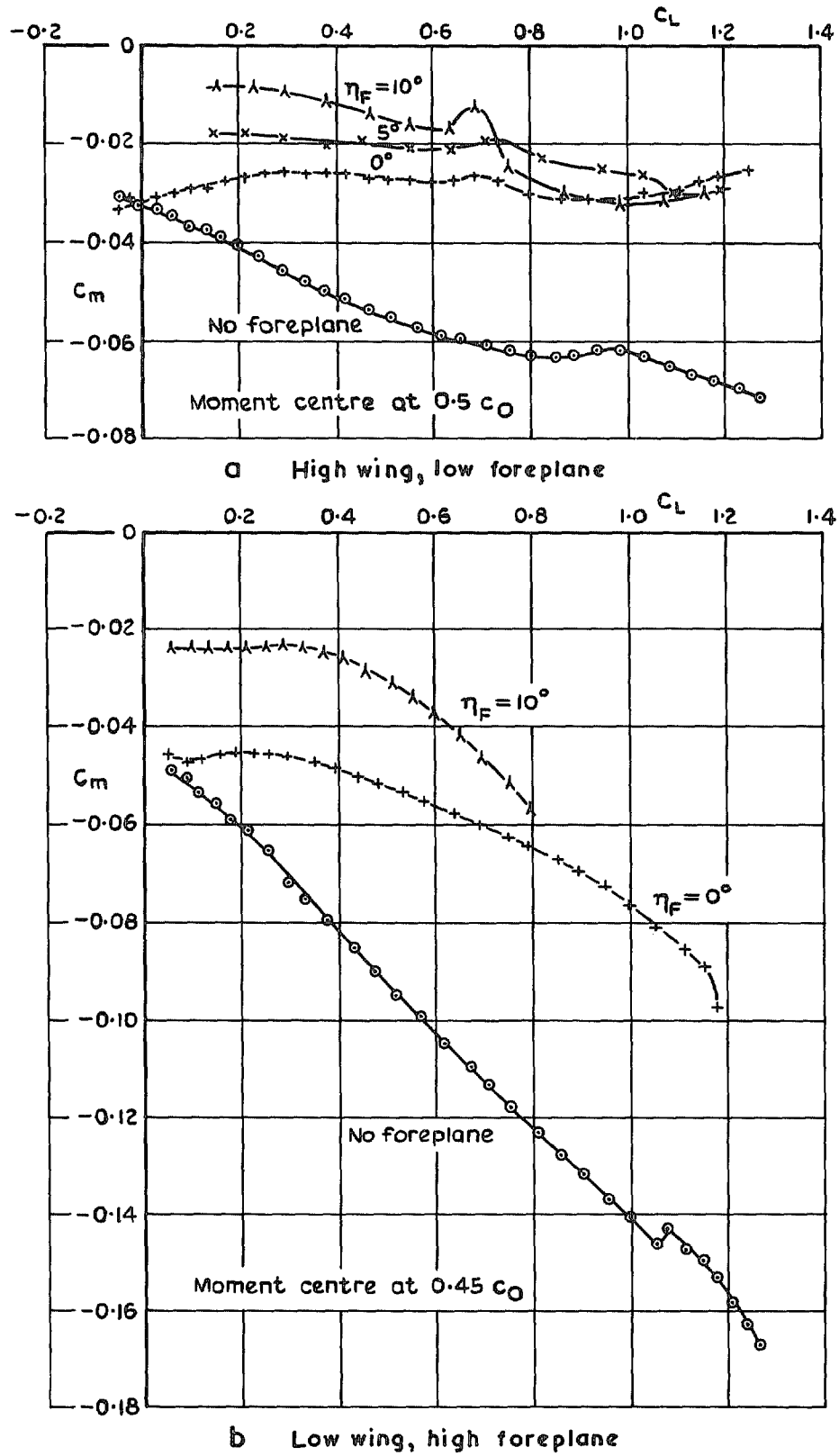

FIG. 27a & b. Pitching moment coefficients with and without a foreplane, trailing edge controls deflected $\eta = 10°$.

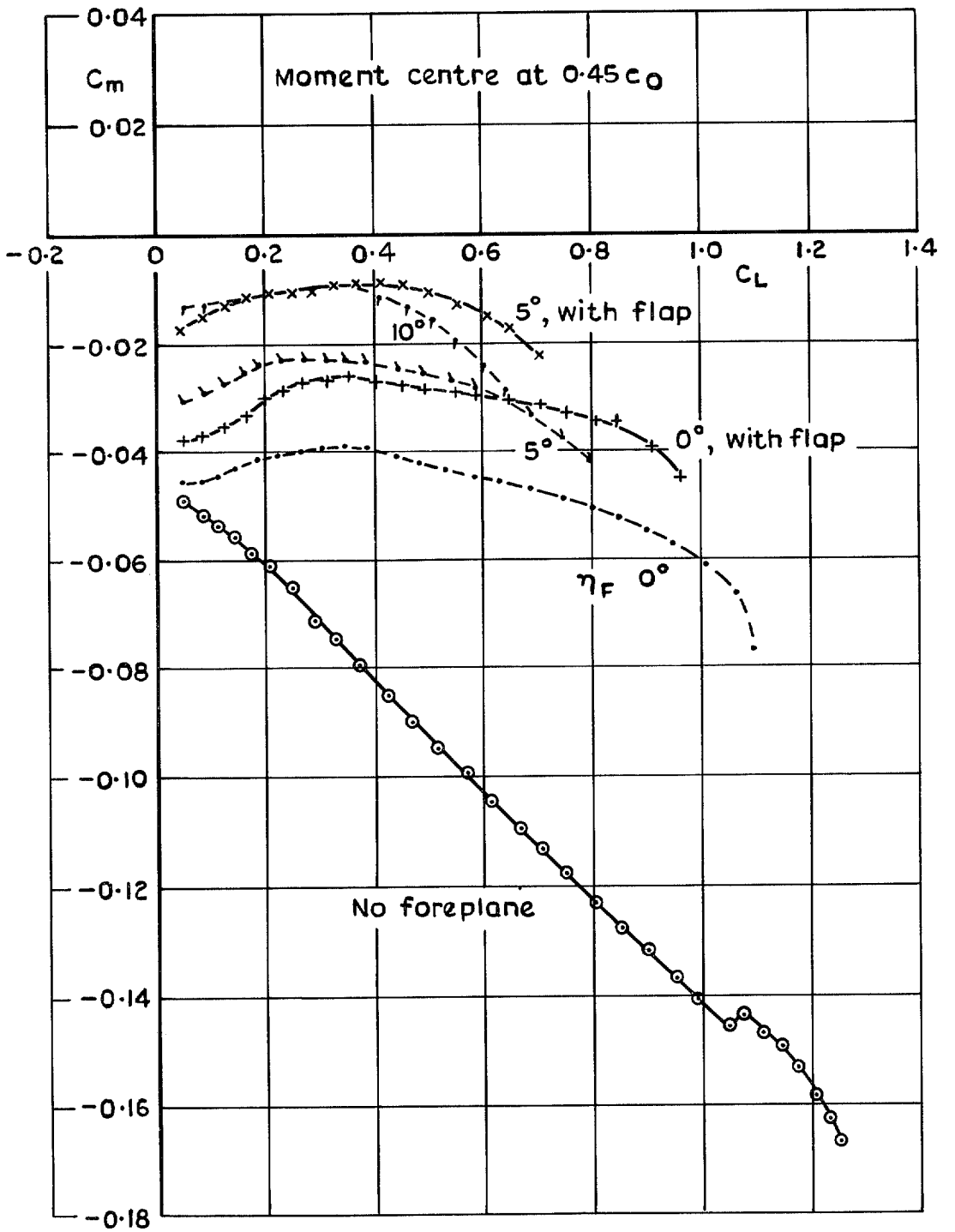

FIG. 28. Pitching moment coefficients with foreplane in forward position. Low-wing, trailing-edge controls deflected, $\eta = 10°$.

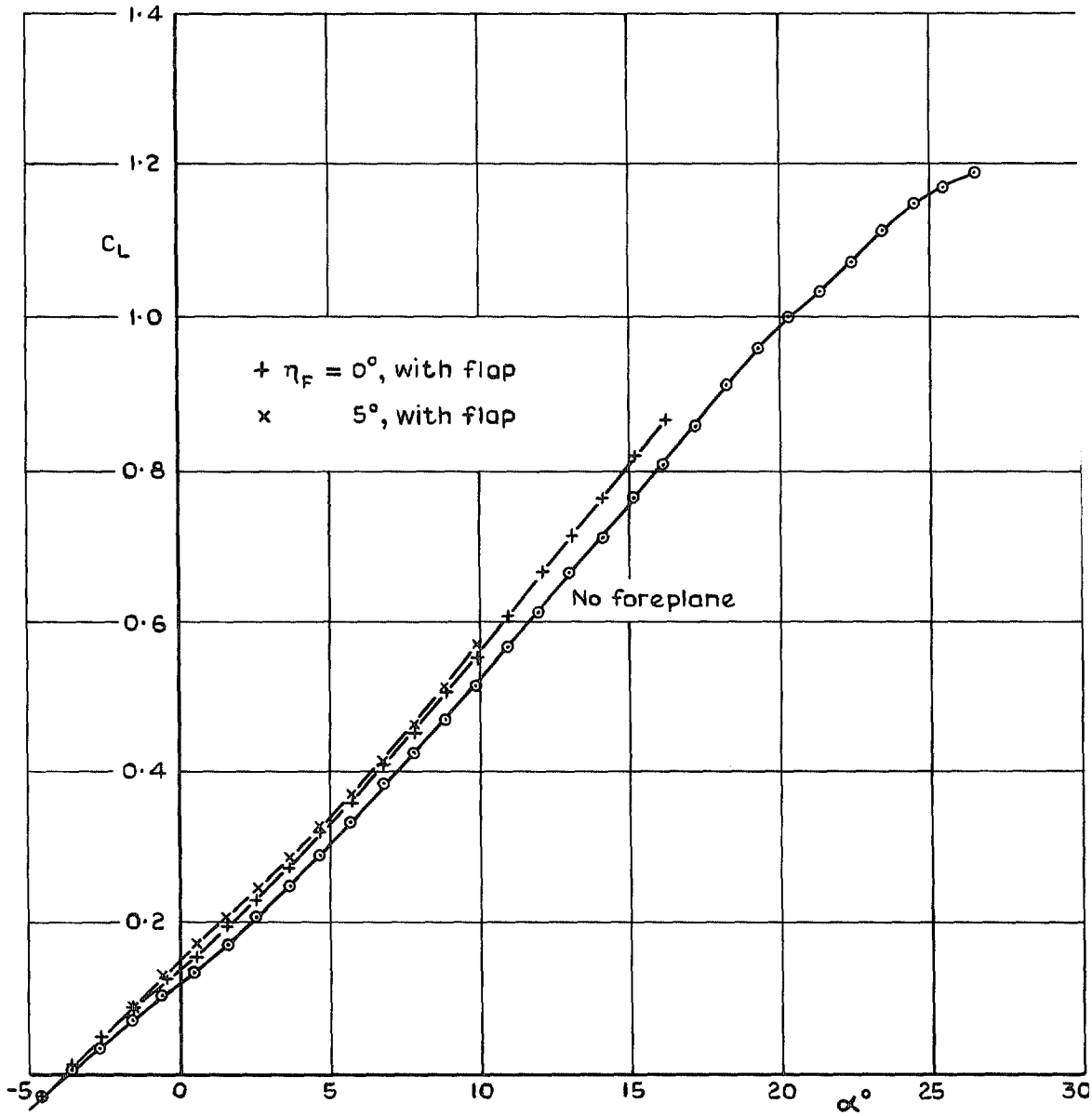

FIG. 29. Lift coefficient with foreplane in forward position. Low-wing, trailing-edge controls deflected. $\eta = 5°$.

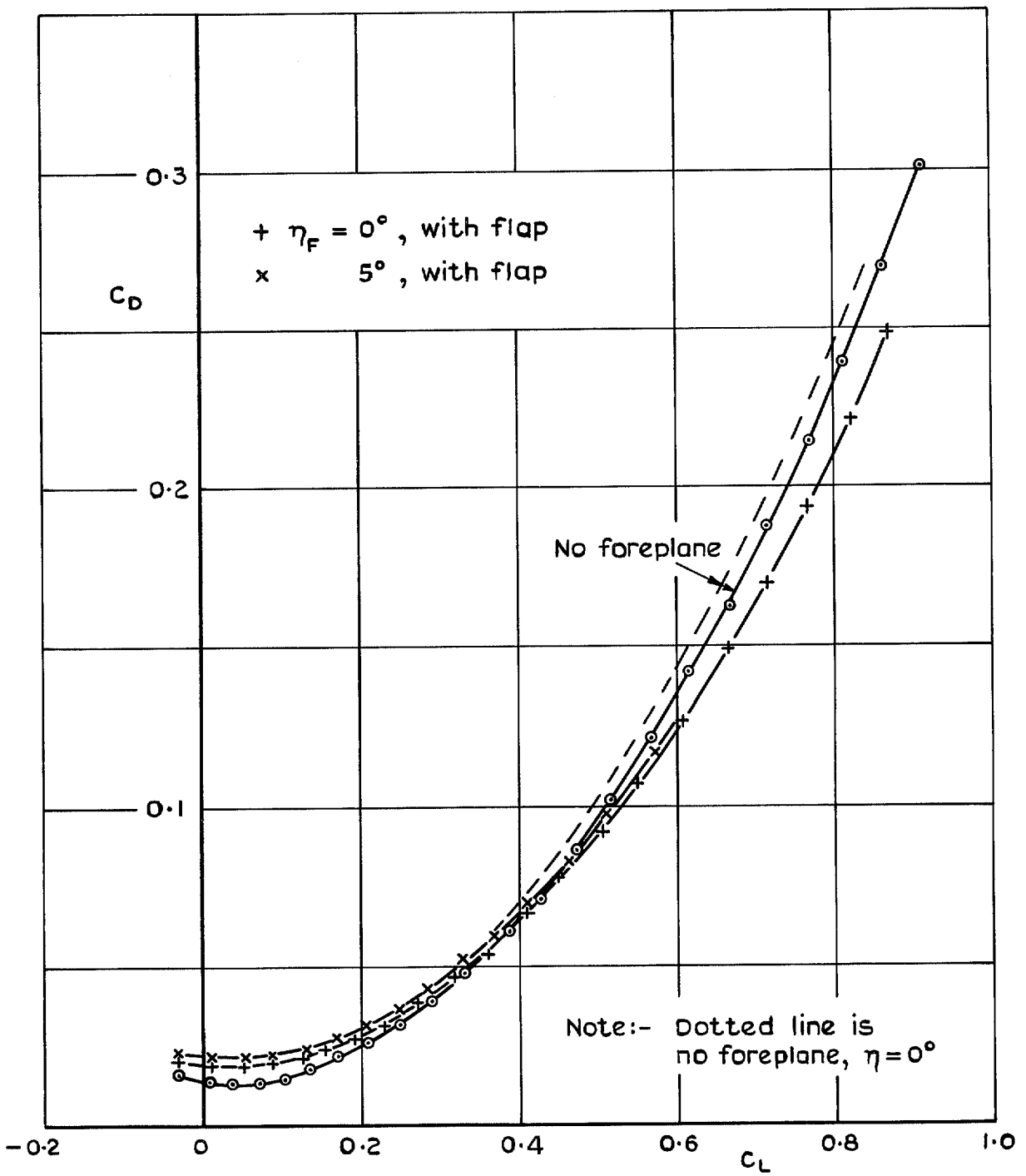

FIG. 30. Drag coefficients with foreplane in forward position. Low-wing, trailing-edge controls deflected, $\eta = 5°$.

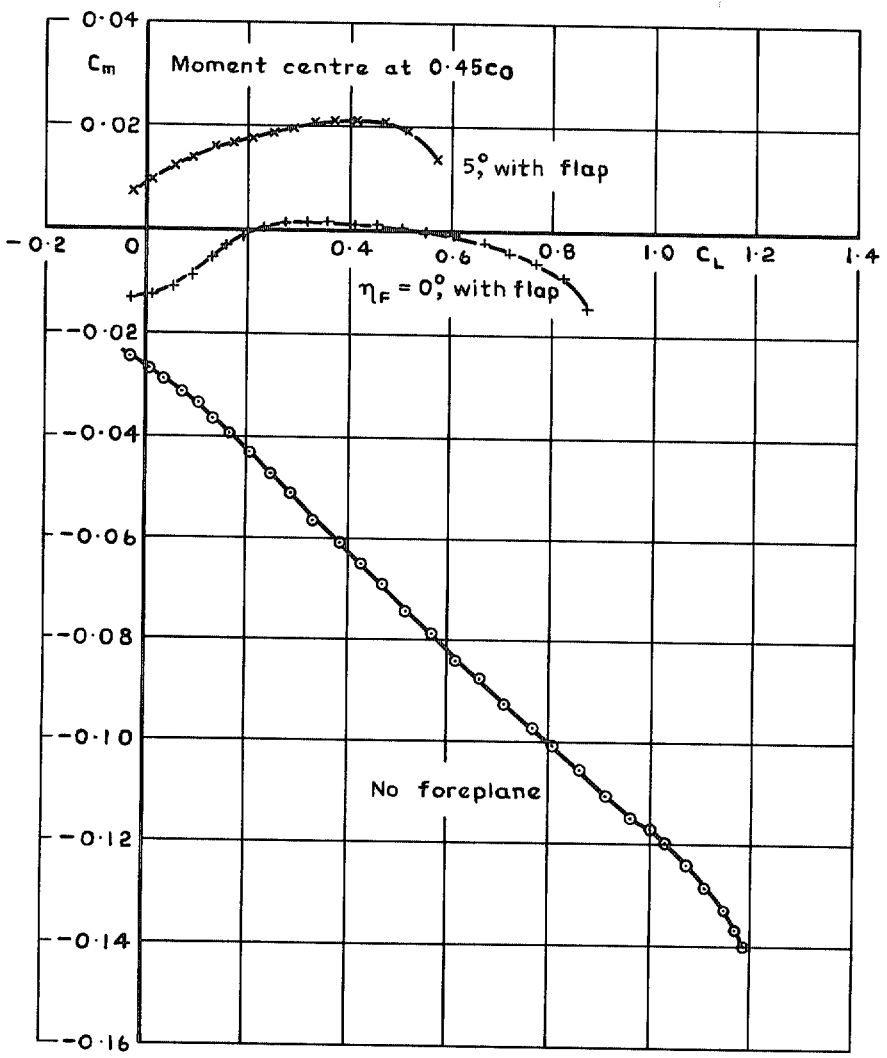

FIG. 31. Pitching moment coefficients with foreplane in forward position. Low-wing, trailing-edge controls deflected, $\eta = 5°$.

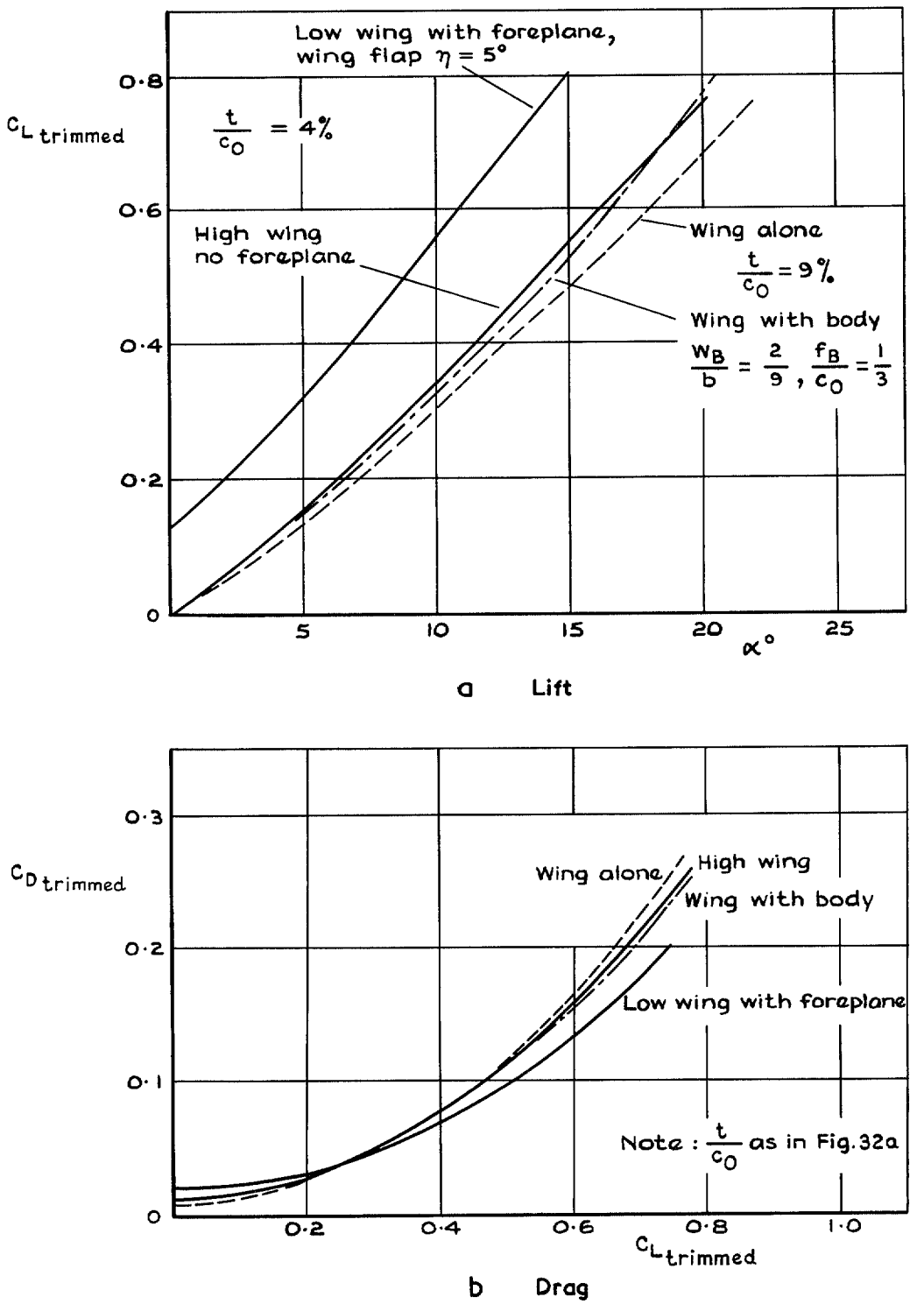

FIG. 32a & b. Trimmed lift and drag coefficients at model Reynolds number $\simeq 2 \times 10^6$.

Printed in England for Her Majesty's Stationery Office by J. W. Arrowsmith Ltd., Bristol BS3 2NT.
Dd. 505715 K5 5/74.

HER MAJESTY'S STATIONERY OFFICE

Government Bookshops

49 High Holborn, London WC1V 6HB
13a Castle Street, Edinburgh EH2 3AR
41 The Hayes, Cardiff CF1 1JW
Brazennose Street, Manchester M60 8AS
Southey House, Wine Street, Bristol BS1 2BQ
258 Broad Street, Birmingham B1 2HE
80 Chichester Street, Belfast BT1 4JY

Government publications are also available through booksellers

ISBN 0 11 470840 1